https://doi.org/10.5194/egusphere-2026-2161
Preprint. Discussion started: 23 April 2026

Measurement report: Chemical composition of submicron aerosol and cirrus and contrail ice residuals measured in the UTLS over Germany in winter 2018

Philipp Brauner[1,*], Oliver Appel[1,*,2], Oliver Eppers[1,*], Franziska Köllner[2,1,*], Hans-Christian Clemen[1,*], Tiziana Bräuer[3], Hans-Christoph Lachnitt[2], Katharina Kaiser[1,*], Johannes Schneider[1,*], Antonis Dragoneas[4], Andreas Hünig[1,8], Sergej Molleker[5], Bruce E. Anderson[6], Yafang Cheng[7,*], Hans Schlager[3], Christiane Voigt[2,3], and Stephan Borrmann[1,2]

[1]Particle Chemistry Department, Max Planck Institute for Chemistry, Mainz, Germany
[2]Institute for Physics of the Atmosphere, Johannes Gutenberg University, Mainz, Germany
[3]Institute of Atmospheric Physics, Deutsches Zentrum für Luft- und Raumfahrt (DLR), Oberpfaffenhofen, Germany
[4]Climate Geochemistry Department, Max Planck Institute for Chemistry, Mainz, Germany
[5]Instrument Development and Electronics Department , Max Planck Institute for Chemistry, Mainz, Germany
[6]NASA Langley Research Center (LaRC), Hampton, USA
[7]Multiphase Chemistry Department , Max Planck Institute for Chemistry, Mainz, Germany
[8]now at: SCHOTT AG, Mainz, Germany
[*]now: Aerosol Chemistry Department, Max Planck Institute for Chemistry, Mainz, Germany

Correspondence: Stephan Borrmann (stephan.borrmann@mpic.de)

Abstract. The knowledge of submicron aerosol composition in the upper troposphere and lower stratosphere (UTLS) and the contribution of aircraft exhaust on the cirrus and contrail formation is still limited due to sparse observations and snapshots not considering the evolution of these clouds. Airborne measurements of the aerosol chemical composition were conducted in the 2018 wintertime UTLS region over Germany. With the help of the hybrid mass spectrometer ERICA (ERC Instrument for the Chemical composition of Aerosols), the composition of background aerosol was analyzed as well as the composition of cloud residuals by applying a counterflow virtual impactor. We found that carbonaceous material plays an important role in the particulate matter in the wintertime UTLS over Germany, among which biomass burning (BB) material is the prevailing species. Complementary simulations of air mass history and synoptical analysis suggest that BB material results from wildfires, in particular the Thomas fire in Northern America. Besides the long-range transport of BB aerosol, the chemical composition of UTLS aerosol is driven by local meteorological conditions. Further, carbonaceous aerosol from aircraft exhaust including soot and engine oil contribute to the aerosol population in the size range below 200 nm. Aging contrails contain signatures of aircraft exhaust such as coated soot and engine oil among other biogenic organic compounds and are consistent with the enhancement of these compounds in aircraft exhaust plumes. Sea spray and mineral dust dominate cirrus residuals, implying the formation at a liquid state.

https://doi.org/10.5194/egusphere-2026-2161
Preprint. Discussion started: 23 April 2026

1 Introduction

The upper troposphere and lower stratosphere (UTLS) describes a transition layer located approximately ± 5 km around the local tropopause (Gettelman et al., 2011). This region is characterized by chemical and dynamical properties of both spheres and faces a complex interplay of clouds, radiation, and deep convection besides large- and small-scale circulation patterns (Gettelman et al., 2011; Randel and Jensen, 2013). Aerosol particles are a significant contributor within the UTLS region and have been the subject of research in this region for 60 years and ongoing. While Junge et al. (1961) and Kremser et al. (2016) focused on stratospheric aerosol, Brock et al. (1995) and Murphy et al. (1998) were the first to analyze UTLS aerosol in particular. Minor changes in the amount of trace gases in the UTLS lead to large changes in the global radiation budget (Riese et al., 2012). Analogously, the importance of aerosols is related to their impact on the radiative forcings of the atmosphere and, thus, on their contribution to global climate change. They interact with solar and terrestrial radiation in a direct way but they can also act as cloud or ice nuclei forming clouds that subsequently redistribute the incoming shortwave and outgoing longwave radiation (Arias et al., 2021). Although a large number of processes in the UTLS region is well understood, the contribution of aerosol particles to cloud formation and the role of both, particles and clouds, in the radiation budget is still subject to considerable uncertainty (Arias et al., 2021).

Aerosol particles in the UTLS region are largely composed of sulfur-containing species, primarily due to oxidation of carbonyl sulfide which has a long tropospheric lifetime and is transported to the UTLS region before being processed. Besides this, volcanic eruptions can directly inject tons of sulfur material into the UTLS and stratosphere (e.g., McCormick et al., 1995; Thomas et al., 2009) affecting the chemical composition (Textor et al., 2004; von Glasow et al., 2009; Poberaj et al., 2011; Aquila et al., 2013) and the global radiative forcing (e.g., Solomon et al., 2011; Santer et al., 2014; Andersson et al., 2015). Sulfuric acid droplets can absorb upwelling longwave radiation (Weisenstein et al., 2022) and scatter the incoming solar radiation back to the outer space, resulting in a cooling of the troposphere (Labitzke and McCormick, 1992; McCormick et al., 1995). In addition to sulfate, further substances have been observed in the UTLS. Large amounts of gases are emitted from ground sources in the boundary layer (BL) before being transported to the UTLS via warm conveyor belts (WCB) or convective uplift (Reutter et al., 2015; Homeyer et al., 2017; Joppe et al., 2025) and subsequently mixed into the lowermost stratosphere (LMS) via cross-isentropic mixing (Woiwode et al., 2018; Kaluza et al., 2021; Tomsche et al., 2022; Voigt et al., 2022; Lachnitt et al., 2023). Recent studies consider a complementary transport path assigned to the Asian summer monsoon (Randel and Park, 2006; Höpfner et al., 2016, 2019; Appel et al., 2022; Eppers et al., 2025) which includes the uplift of pollutants from the Asian boundary layer via monsoon convection into the UTLS region, a trapping of these air masses inside the Asian Monsoon Anticyclone (Randel and Park, 2006; Höpfner et al., 2016, 2019), and a subsequent entrainment into the northern hemisphere UTLS region by eddy shedding (Ploeger et al., 2012; Vogel et al., 2014; Wang et al., 2022). Within the monsoon system, aerosol particles of boundary layer origin are removed by wet deposition during convective uplift but trace gases continue their way to the tropopause region where they form the Asian Tropopause Aerosol Layer (Höpfner et al., 2016; Appel et al., 2022). The secondary aerosol particles are formed by oxidation and subsequent condensation of substances such as nitric and sulfuric acid as well as low-volatile organic compounds, known as gas-to-particle conversion (Myhre et al., 2013).

https://doi.org/10.5194/egusphere-2026-2161
Preprint. Discussion started: 23 April 2026

Another transport mechanism for aerosol particles into the stratosphere is provided by the Brewer-Dobson circulation (BDC): air masses are uplifted from the tropical upper troposphere to the stratosphere where they are distributed along the lower or upper stratospheric branch before they start to descend at mid and high latitudes into the UTLS region. Quasi-isentropic mixing enables the transport of particles from the tropical tropopause layer towards the LMS and vice versa (Kremser et al., 2016; Kunkel et al., 2019; Martinsson et al., 2019). The chemical composition of the UTLS aerosol is matter of current research (e.g., Martinsson et al., 2019; Brock et al., 2021).

Intensive wildfires have raised recent attention as they appeared more frequently within the last decade (e.g., Franklin et al., 2014; Jolleys et al., 2015; Sakamoto et al., 2015). These forest fires trigger severe thunderstorms and support the ascent of biomass burning plumes within pyro-convective clouds (Fromm and Servranckx, 2003; Damoah et al., 2006; Ditas et al., 2018; Yu et al., 2019). Large amounts of smoke particles are lifted and enter the UTLS region. Although these particles may act as cloud condensation nuclei or ice nucleating particles during the uplift, the number of smoke particles is so large that the majority continues its way into the lower stratosphere as interstitial aerosol (Baars et al., 2019). Once taken to the stratosphere, the smoke particles are transported along the jet stream and subsequently distributed across the entire hemisphere. The particles remain in the UTLS region for months, thereby affecting aerosol optical thickness and the extinction of radiation (e.g., Baars et al., 2019; Yu et al., 2019). However, the knowledge of the contribution of biomass burning material to the UTLS particulate matter is still unclear.

Besides the transport of aerosol particles or precursor gases towards the UTLS region, in situ aircraft emissions have a manifold impact on the tropopause region. The particulate matter attributed to aviation includes ultra-fine soot, organic, and sulfate particles (Moore et al., 2017; Dischl et al., 2024, 2025) as well as ultra-fine metal pieces which are traced back to kerosene, engine lubrication oil, or engine wear. In cold and humid ice-supersaturared conditions, these compounds support ice nucleation in condensation trails (contrails) as well as cirrus clouds (Agrawal et al., 2008; Abegglen et al., 2016). Further, aircraft emit greenhouse gases such as CO_2 and water vapor of which the latter contributes to the formation of contrails (Voigt et al., 2021). Suitable conditions for contrail formation are reached when hot aircraft engine exhaust is mixed with cold and dry ambient air in the wake vortex, providing supersaturation with respect to water (Bräuer et al., 2021a). The emitted water vapor rapidly condenses onto soot and other aerosol particles, resulting in small water droplets (Kärcher, 2018), that immediately grow in size and tend to freeze if the ambient air is supersaturated with respect to ice (Heymsfield et al., 2010; Bräuer et al., 2021a). The impact of contrails on global climate change is significant as they scatter incoming solar radiation and absorb outgoing longwave radiation similar to cirrus (Burkhardt and Kärcher, 2011; Boucher et al., 2013). The global effective radiative forcing (ERF) ranges between 17 and 98 $\mathrm{mW\,m^{-2}}$, i.e. the mean net effect is warming and of similar magnitude as the ERF by all aircraft CO_2 emissions since the historical start of aviation in the 1940s (Lee et al., 2021). Contrail research is of major interest as the ERF already increased by 48 % between 2005 and 2018 due to an intensifying global air traffic. As global aviation is expected to triple until 2050 (Bock and Burkhardt, 2019), mitigation strategies are needed to reduce contrail formation. Besides the detour of aircraft routes to areas where warming contrails would form, the research focuses on the reduction of aircraft emissions, mainly soot, by changing the jet fuel composition (Moore et al., 2017; Kärcher, 2018; Voigt et al., 2021; Märkl et al., 2024; Voigt et al., 2025). Although soot has been found to largely affect the ice crystal numbers inside contrails, a

https://doi.org/10.5194/egusphere-2026-2161
Preprint. Discussion started: 23 April 2026

scan of the chemical composition of contrails has not been provided yet. Further, the impact of aerosol chemical composition on contrail formation is still subject of current research.

Besides their contribution to contrails, aerosol particles also support the formation of cirrus clouds and determine their physico-chemical properties. Cirrus clouds cover about 30 % of the midlatitude UT (Wylie and Menzel, 1999) and lead to cooling or warming of the global climate depending on their formation process (Krämer et al., 2020), chemical composition, physical parameters such as size, shape, and surface roughness as well as the Earth's surface and atmosphere (Liou, 1986; Tang et al., 2017). Naturally, the formation of most cirrus clouds is linked to ascending air masses on mesoscale or large-scale via frontal systems, ridges, jet streams, lee waves, or convection (Gayet et al., 2012; Krämer et al., 2009; Lawson et al., 2006; Muhlbauer et al., 2014; Stith et al., 2014; Jackson et al., 2015; Heymsfield et al., 2017; Voigt et al., 2017). In order to characterize cirrus clouds, ice water content (IWC, Schiller et al., 2008; Krämer et al., 2016, 2020), ice crystal number and size (Krämer et al., 2009, 2016, 2020), as well as relative humidity including supersaturation with respect to ice are considered (Jensen et al., 2005; Kaufmann et al., 2016). Based on the updrafts during the ice nucleation process, cirrus clouds can be separated into liquid-origin (10^{-3} to $1\,\mathrm{g\,m^{-3}}$) and in situ-origin (10^{-7} to $10^{-2}\,\mathrm{g\,m^{-3}}$), also differing in IWC, ice crystal size and thickness (Luebke et al., 2016). Mineral dust is predominant in 75 % to 93 % of all cirrus crystals (Cziczo et al., 2013; Twohy, 2015; Kanji et al., 2017; Froyd et al., 2022), and thus a major contributor to cirrus formation among other species such as anthropogenic metals (Cziczo et al., 2004, 2013; Cziczo and Froyd, 2014) and sea spray particles (Cziczo et al., 2013; Patnaude et al., 2024). Further compounds detected within cirrus ice crystals comprise ammonium sulfate, secondary organic aerosols, and black carbon, of which the latter rather contributes in case of prior cloud processing (Mahrt et al., 2018, 2020).

Despite the focus on few individual particle types and transport processes towards the UTLS region, detailed and comprehensive observations of the UTLS aerosol composition above Europe are still sparse. Here, in situ airborne measurements are required to improve our understanding of the influence of aerosol chemical composition on cirrus cloud and contrail formation. In this study, we present airborne measurements of the ND-MAX campaign 2018 and gain insights to the wintertime UTLS submicron aerosol chemical composition over Germany using two different methods combined in a novel hybrid aerosol mass spectrometer. We identify individual particle types occurring in the UTLS background aerosol population and try to assign the particle types of aircraft origin. Further, we investigate the potential source regions and meteorological processes that contribute to the aerosol population based on few examples. Then, we analyze the cloud residuals of cirrus and contrails to gain insights to the formation process of cirrus in particular, and to characterize the particle types involved in the formation process of both, cirrus and contrails.

2 Campaign and instrumentation

2.1 ND-MAX aircraft campaign

The particle composition measurements were conducted within the"NASA and DLR Multidisciplinary Airbone eXperiments" (ND-MAX) which were part of the "Emission and Climate Impact of Alternative Fuels" (ECLIF-II) project. The collaborative campaign between the US American National Aeronautics and Space Administration (NASA) and the German Aerospace

https://doi.org/10.5194/egusphere-2026-2161
Preprint. Discussion started: 23 April 2026

Center (Deutsches Zentrum für Luft- und Raumfahrt, DLR) was placed at the NATO and US Air Base Ramstein, Germany (Voigt et al., 2021). The research campaign was conducted using two aircraft: The NASA DC-8 aircraft contained a comprehensive suite of physicochemical aerosol analysis instruments, trace gas and cloud instruments and recorded meteorological parameters. The "Advanced Technology Research Aircraft" (ATRA) of the DLR was used as source aircraft to produce exhaust and contrails which had subsequently been measured with the instrumentation onboard the NASA DC-8 aircraft. For this purpose, the DLR-ATRA was fueled with various mixtures of standard kerosene type Jet A-1 and bio-based alternative jet fuel (Bräuer et al., 2021b, a; Voigt et al., 2021). Due to the cut-off particle size of the ERICA mass spectrometer at $\sim 170\ \mathrm{nm}$ (d_{50}), the characterization of aerosols from individual fuel blends is beyond the scope of this analysis. The DLR-ATRA, its exhaust plume, and the contrails were followed by the NASA DC-8 aircraft. Airborne field measurements were taken in two restricted air space areas over Northern Germany, both close to the sea side (Fig. 1) at three distinct flight levels of 26000, 32000, and 38000 ft (approximately 7.9, 9.8, and 11.6 km, respectively). All together, eight research flights (RFs) were conducted between 17 January and 1 February 2018 including more than 44 flight hours, see also Bräuer et al. (2021a). The goal of the campaign was to investigate the effects of alternative fuel blends on aircraft soot emissions and their impact on climate-relevant properties of the resulting contrail cirrus clouds (Bräuer et al., 2021b; Voigt et al., 2021; Schripp et al., 2022). However, the RFs also provided the opportunity to measure the UTLS background composition as well as cirrus clouds at the corresponding flight levels. This allows us to analyze the recorded data with regard to the aerosol chemical composition and its contribution to the formation of cirrus and contrails.

2.2 ERICA measurements and complementary measurements

The measurements of the aerosol chemical composition were conducted using the hybrid mass spectrometer ERICA (ERC Instrument for the Chemical composition of Aerosols; Hünig et al., 2022; Dragoneas et al., 2022) which consists of two individual mass spectrometers, the ERICA-LAMS and ERICA-AMS. The ERICA-LAMS (laser ablation mass spectrometer) is based on the laser desorption and ionization technique (LDI) and a subsequent time-of-flight mass spectrometer (TOF-MS) (e.g., Hinz et al., 1994; Prather et al., 1994; Murphy and Thomson, 1995; Zelenyuk and Imre, 2005). The instrument is used for the analysis of single particles in a size range of 170 nm to 3.2 µm. The ERICA-AMS implements the thermal desorption and ionization technique (TDI) for bulk measurements of ensembles of particles ranging from 80 nm to 2 µm (Hünig, 2020). The method was first deployed in the Aerodyne AMS and is described in Drewnick et al. (2005) and Canagaratna et al. (2007). Both mass spectrometers share one vacuum chamber, allowing for the parallel sampling of the same air mass. The hybrid system was introduced in detail by Hünig et al. (2022) and Dragoneas et al. (2022). A brief description is provided in the supplement, Sect. S1.

In total, 54403 mass spectra of single particles were recorded with ERICA-LAMS throughout the ND-MAX campaign (except for RF7). Of the detected mass spectra, 52134 spectra refer to aerosol particles measured under cloud-free conditions using the scoop inlet (Sect. 2.3). 2269 mass spectra were sampled through a CVI (Sect. 2.3) and are assigned to cloud particle residuals (CPRs). Due to a leakage in the inlet line, the single-particle data of RF7 were disregarded. The raw mass spectra were processed using the software package CRISP (Concise Retrieval of Information from Single Particles; Klimach, 2012). After a

https://doi.org/10.5194/egusphere-2026-2161
Preprint. Discussion started: 23 April 2026

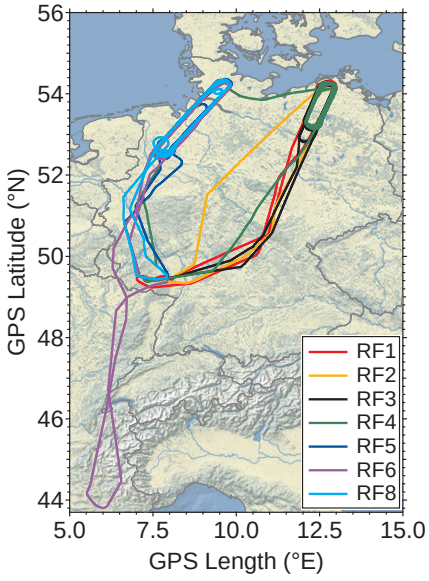

Figure 1. Map of the considered research flights of ND-MAX in winter 2018. The solid lines (colored by different research flights (RF)) demonstrate the flight paths of the NASA DC-8 aircraft. The two elongated, oval shaped flight patterns over Northern Germany are located in the two restricted air space areas (7.5°–10.0° E and 11.5°–13.0° E, both 52.5°–54.5° N) that were used for the tracking of the ATRA. The map was created with data from Natural Earth.

m/z (ion mass-to-charge ratio) calibration and peak area integration, the particles were classified by a fuzzy c-means clustering algorithm (Hinz et al., 1999; Roth et al., 2016; Schneider et al., 2021). A description of the clustering routine is provided in Sect. S2. In total, 14 individual types are obtained including carbonaceous compounds (elemental carbon (EC)/soot, coated soot, biomass burning (BB), processed elemental and organic carbon (ECOC), processed organic carbon (OC), amines as well as engine oil) and inorganic material (sea spray, processed sea spray, mineral dust, processed mineral dust, a nitrogen-rich type, and meteoric material). A detailed description of all particle types obtained by this routine including their characteristic ion marker peaks is provided in Tables S2 and S3. In addition, a mean mass spectrum is provided for every particle type (Fig. S1 to S12). For this study, only the relative abundance of individual particle types is considered in terms of particle fraction, i.e., the number of single particles attributed to a certain particle type divided by the number of all analyzed particles.

The ERICA-AMS data were analyzed using the data analysis tool TofWare 2.5.7 (Tofwerk). The detection limits of the mass concentrations are computed based on the closed signal with the Savitzky-Golay procedure (Savitzky and Golay, 1964) to detrend the signal. A detailed description of the analysis tool and the processing with Savitzky-Golay is provided in the supplement of Appel et al. (2022). The detection limits during ND-MAX were found to be 0.63 $\mu g\,m^{-3}$ for ammonium, 0.11 $\mu g\,m^{-3}$ for nitrate, 0.43 $\mu g\,m^{-3}$ for organic, 0.07 $\mu g\,m^{-3}$ for sulfate, and 0.08 $\mu g\,m^{-3}$ for chloride and refer to a sampling period of 10 s consisting of aerosol and background measurement (with closed shutter) of 5 s duration each. These values are comparable to those determined for the StratoClim aircraft campaign 2017 under the same configuration (Appel et al.,

https://doi.org/10.5194/egusphere-2026-2161
Preprint. Discussion started: 23 April 2026

Table 1. ND-MAX instrumentation consulted in this study in addition to mass spectrometry.

Instrument	**Target parameter**	**Accuracy (A)/ Precision (P)/ Uncertainty (U)**	**Data frequency**	**Reference**
CPC model 3010 by TSI Instruments	Aerosol number concentration of particles in a size range of 10 to 3000 nm (normalized to standard temperature (273.15 K) and pressure (1013.25 hPa)	A: 15 %	1 Hz	Bräuer (2021); Bräuer et al. (2021b)
Laser Aerosol Spectrometer (LAS) model 3340 by TSI Instruments	Aerosol particle concentration and size distribution in a range of 90 to 7500 nm	P: 5 %	1 Hz	Moore et al. (2021); TSI (2017)
Cavity Ring Down Spectroscopy (CRDS, model: G2301-m) by Picarro	CO_2 volume mixing ratio	A: 0.3 ppmv	0.5 Hz	Bräuer (2021); Bräuer et al. (2021b); Voigt et al. (2021)
Fast Forward Scattering Spectrometer Probe (FFSSP)	Ice particle number concentration in a size range of 1 to 25 µm	A: 10–35 %	1 Hz	Baumgardner et al. (1992); Brenguier et al. (1998); Bräuer et al. (2021b)
Cloud Imaging Probe by Droplet Measurement Technologies	Cloud particles in a size range of 15 to 900 µm	U: 20 %	1 Hz	Baumgardner et al. (2001); Klingebiel et al. (2015); DMT (2014)

2022) and those shown by Hünig et al. (2022). The analysis of the ERICA-AMS data revealed an inconsistency of the mass concentrations measured during RF6. In consequence, RF6 was excluded from the ERICA-AMS data. Further, the data of RF7 were not included in this analysis due to a leakage of the ERICA instrument.

In addition to the aerosol chemical composition, the comprehensive suite of instruments aboard the NASA-DC8 measured trace gases, water vapor, and the chemicophysical properties of aerosol particles. Table 1 provides an overview of the instrumentation consulted for this study.

https://doi.org/10.5194/egusphere-2026-2161
Preprint. Discussion started: 23 April 2026

2.3 Scoop inlet and counterflow virtual impactor

A scoop-type air intake system (Almeida et al., 2021; Anderson et al., in prep.) was deployed to sample aerosol particles up to 1 µm in size. The scoop inlet was mounted on the forward zenith port of the NASA DC-8 and tapered from the inlet towards the exhaust in order to provide a boost in ram pressure (Anderson et al., in prep.). Within this study, measurements at the scoop inlet were disregarded in the presence of clouds. The sample is introduced and guided through a probe towards a manifold which contains a sample extraction orifice. Before reaching the sample extraction tube, a deflector separated supermicron particles from the sample flow in order to provide submicron particles to the aerosol instruments (Moore et al., 2004; Voigt et al., 2021; Anderson et al., 2015).

The inlet for sampling of cloud residuals was a Counter-flow Virtual Impactor (CVI) from Brechtel Manufactoring Incorporated (BMI Model 1204, Hayward, CA, USA), which was mounted in a starboard side window of the NASA DC-8. Cloud particles larger than approximately 5 µm in size were collected, evaporated, and enriched by a factor of 8 in minimum above ambient concentrations due to a sub-isokinetic inlet flux, and distributed to ERICA and additional instruments for particle detection and sizing (Anderson et al., in prep.). A detailed description of the working principle is provided by Shingler et al. (2012). In brief, large and inert cloud residuals of the sample air entering the probe-tip overcome a counterflow, whereas small and interstitial particles are rejected. The cloud residuals evaporate under warm and dry ambient conditions inside the CVI tubing and the residual cores are guided towards the research instruments. Large-sized droplets ($d_{droplet} > 40$ µm) impact in an extended region. Interstitial aerosol of particle diameters larger than 5 µm might pass the CVI inlet as well. However, we expect the impact of interstitial particles to be negligible as the their majority would impact in the extended region or inside the tubing.

2.4 Definition of particle-related events

During ND-MAX, we sampled under different conditions and behind two different inlets (see Sect. 2.1 and 2.3). Aerosol particles were detected in the absence of clouds via the scoop inlet, whereas the cloud residuals were sampled through the CVI, including residuals of mixed-phase and ice clouds. In the following, we will differentiate between four measurement conditions (events) at the two sample inlets which are characterized based on complementary measurements of aerosol and ice particle number concentrations as well as CO_2. A detailed description of the definition of these events is provided in Sect. S3. In summary, exhaust plumes (1) are characterized by an enhanced aerosol number concentration and amount of CO_2 above the atmospheric background (2). Both events are based on measurements via the scoop inlet. Natural cirrus clouds (3) are defined by an enhanced ice particle number concentration and a CO_2 level referring to the atmospheric background. Further, the number concentration of aerosol particles was enhanced within cirrus clouds, probably due to ice crystal shattering and the release of absorbed aerosol particles during the ice crystal growth. This enhancement of aerosol particle concentration is used as a second indicator to determine periods of cirrus clouds. However, the processes leading to such an enhancement are still unclear and need further research. An enhanced aerosol number concentration and amount of CO_2 along with an increase of

https://doi.org/10.5194/egusphere-2026-2161
Preprint. Discussion started: 23 April 2026

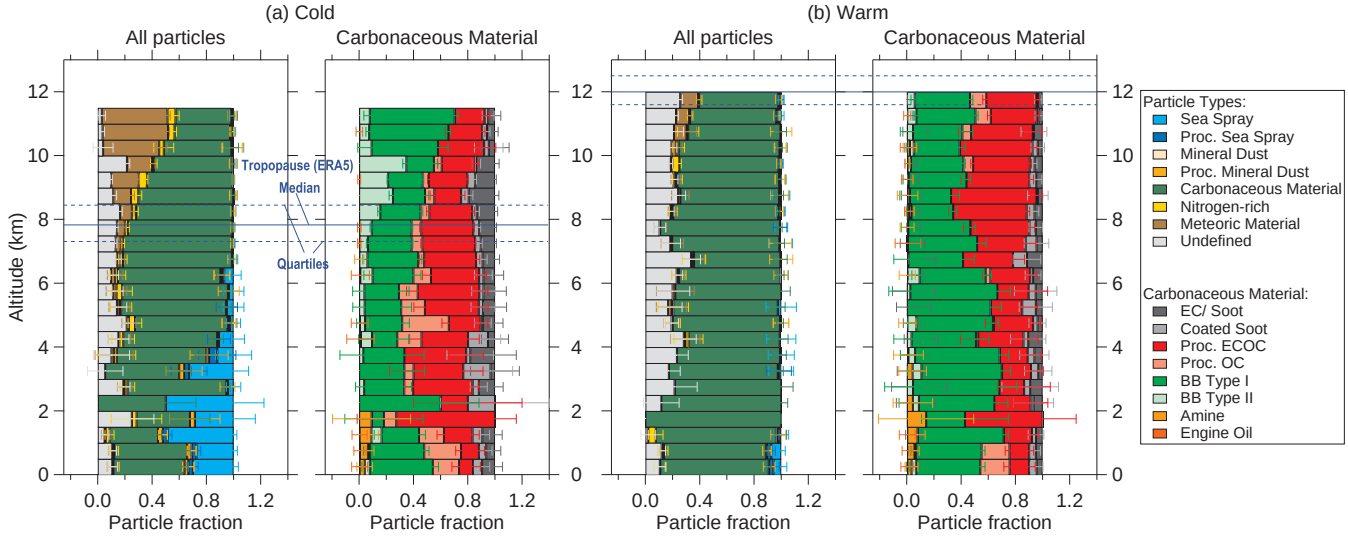

Figure 2. Vertical profile of relative particle type abundance measured at the scoop inlet for the cold (a) and warm (b) period regarding all particle types and the particle types attributed to carbonaceous material broken down. The error bars illustrate the uncertainty of the particle fraction as a result of the binomial counting statistics (Sect. S7). The dashed horizontal lines indicate the tropopause median and percentiles derived from ERA5 data for the cold and warm period (Hersbach et al., 2018).

ice particle number concentration implies the presence of a contrail (4). Both, cirrus and contrails, were sampled using the CVI and filtered for temperatures below -38 °C in order to exclude liquid or mixed-phase clouds.

3 Results

We analyzed the particle chemical composition of the wintertime tropopause region and lowermost stratosphere over Germany based on our ERICA-LAMS and ERICA-AMS measurements. The ERICA-AMS recorded mass concentrations of the non-refractory species, supporting the determination of potential particle source regions and emitters while the ERICA-LAMS provided information on the chemical composition on a qualitative base including refractory and non-refractory material. The measurements were attributed to a cold and warm period, depending on the prevailing meteorological conditions. In brief, the cold period was characterized by a lowered tropopause at approximately 8 km, descending air masses and a northwestern circulation. In contrast, the warm period was characterized by pre-frontal meteorological conditions such as ascending air masses and the advection of warm tempered air masses towards the flight area were observed along with an up-level tropopause around 12 km (Sect. S5).

https://doi.org/10.5194/egusphere-2026-2161
Preprint. Discussion started: 23 April 2026

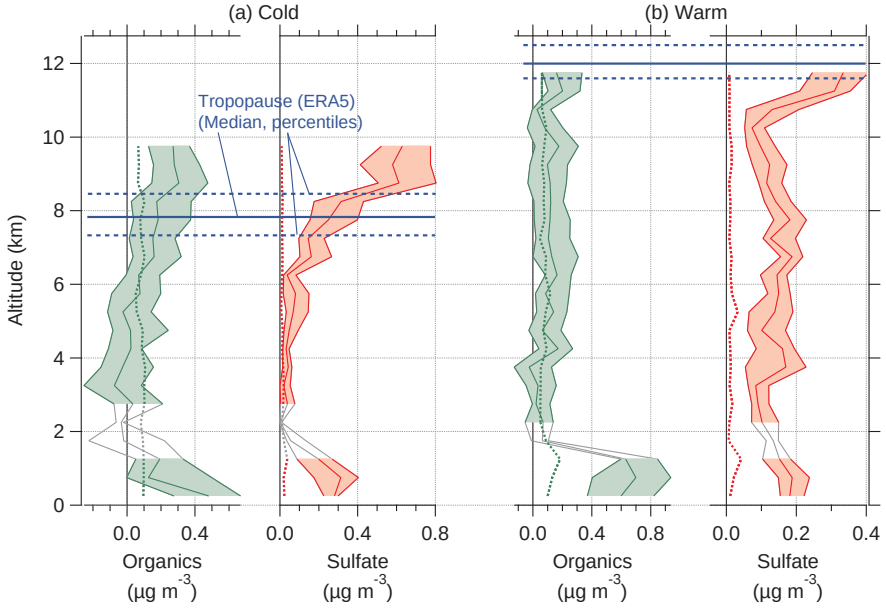

Figure 3. Vertical profiles of mass concentrations of particulate organics (green) and sulfate (red) obtained by the ERICA-AMS as a function of GPS altitude for the cold period (a, RF1, RF2, and RF8) and warm period (b, RF3 and RF4) of the ND-MAX campaign 2018, binned in 500 m steps. The profiles refer to aerosol measurements via the scoop inlet. The solid line and the shaded area represent the median and quartiles. For each altitude bin and substance the detection limit is displayed as a dotted line. The altitude range between 1.5 and 2.5 km in the cold period (between 1.5 and 2.0 km in the warm period) is not shaded since these bins comprise low counting statistics, i.e. less than 10 counts per bin. The horizontal lines indicate the tropopause median and quartiles derived from ERA5 data for the cold and warm period (Hersbach et al., 2018).

3.1 The dominance of carbonaceous particles in the winter UTLS region over Germany

Carbonaceous, meteoric, and sulfate aerosol in the wintertime UTLS

Carbonaceous material dominates the particulate matter in the wintertime UTLS region over Germany. Figure 2 presents the individual particle types and their occurrence during the cold (a) and warm (b) period of ND-MAX in terms of particle fraction. Figure 2 includes all particles detected by ERICA-LAMS via the scoop inlet, not distinguishing between aircraft exhaust and atmospheric background as the chemical composition between atmospheric background and aircraft exhaust is similar for particles larger than 200 nm as will be shown in Sect. 3.2.

Here, we focus on the cold period because the aircraft did not scan the entire vertical range of the UTLS during the warm period. Up to 80 % of all particles detected are attributed to carbonaceous material. Among them, the largest fraction is provided by the group of BB particles, ranging between 38 % and 70 % (Fig. 2a). Another dominant particle type is the internal mixture of processed ECOC with a fraction up to 39%. Further types containing carbonaceous material are fresh and coated soot that reveal a common fraction between 8 % and 25 % and processed OC reaching up to 8 % in the UT. The enhancement

https://doi.org/10.5194/egusphere-2026-2161
Preprint. Discussion started: 23 April 2026

in organic material in the UT is also observed in the AMS data. Figure 3 provides a vertical profile of the mass concentrations of organics and sulfate obtained by the ERICA-AMS for the cold (a) and warm (b) period of ND-MAX. Concerning the cold period, the vertical profile of organic aerosol displays an increasing mass concentration with increasing altitude, particularly for lower stratospheric air masses.

The LMS is characterized by the predominance of particles containing meteoric material as well as carbonaceous aerosol. The fraction of meteoric particles (Fig. 2a) increases towards the stratosphere, whereas the carbonaceous particle fraction decreases in the same altitude range, still being a dominant class of particles. The mass concentration of organic particulate matter remains on an enhanced level of mass concentration compared to the UT, reaching a local maximum of 0.30 $\mu g\,m^{-3}$ above the local tropopause (Fig. 3a). Moreover, sulfate largely contributes to the LMS. As Fig. 3 reveals, the mass concentration of sulfate is significantly increasing from 0.15 $\mu g\,m^{-3}$ in the UT to approximately 0.60 $\mu g\,m^{-3}$ above the tropopause layer which are in a comparable range to airborne measurements conducted over Central Europe in the UTLS region using a separate C-ToF-AMS during a different campaign (Sect. S6). The predominance of organic and sulfate particles is also observed in the uppermost altitude bins during the warm period (Fig. 2b and 3b). However, the tropopause was located at approximately 12 km and, thus, above the maximum altitude range covered by the research flights. In consequence, the enhancement in the particle fraction of BB particles and mass concentration of organic particles in the LMS is only observed during the cold period. The vertical profiles of ammonium, chloride, and nitrate did not show a clear trend in the UTLS region and are analyzed in Sect. S6.

Biomass burning material in the wintertime UTLS

We analyzed two different types of BB particles of similar chemical signature, mainly differing in the occurrence at different altitude levels and in their particle size. The particles of BB Type I were detected from the ground to the LMS whereas BB Type II was measured within an altitude range between 4 and 11.5 km, with an enhanced particle fraction particularly between 8 and 10 km (Fig. 2a). The size distribution of the ambient particles observed with the ERICA-LAMS at the scoop inlet during the entire campaign is shown in Fig. 4. BB Type I is significantly smaller than BB Type II, implying less aerosol processing and growth compared to BB Type II. In detail, the particles of BB Type I range between 150 and 800 nm, whereas particles of BB Type II are mostly detected in a size range between 500 and 1500 nm. The mean mass spectra of both particle types, BB Type I and BB Type II, facing cation and anion signals are provided in Fig. 5. The chemical signature of both particle types is similar, indicated by the same ion marker peaks. Both mass spectra reveal ion marker peaks of potassium ($m/z+39/41$ (K^+)), nitrate ($m/z-46$ (NO_2^-),-62 (NO_3^-)), sulfate ($m/z-81$ (HSO_3^-),$-97/-99$ (HSO_4^-)) and minor peaks of carbon ($m/z+12$ (C^+),$+24$ (C_2^+)) and sodium ($m/z+23$ (Na^+)) which reveal a biomass burning origin (Pratt et al., 2009; Pratt and Prather, 2010; Schill et al., 2020). The mass spectra indicate that BB Type II is more processed than BB Type I as it contains larger ion peak signals of secondary material such as nitrate (with the exception of $m/z+30$ (NO^+)) and sulfate (Fig. 5, blue sticks). On the other hand, the mean spectrum of BB Type II shows higher signals of BB material compared to BB Type I (Fig. 5, green sticks). The signals of C_2H^- ($m/z-25$) and CNO^- ($m/z-42$) are only included in the mean mass spectrum of BB Type II (Fig. 5, green sticks). Also, the signal of CN^- ($m/z-26$) is larger in the mass spectrum of BB Type II compared to BB Type I. It remains unclear if this signature relates to the coating process or to a different BB source. Regarding their oxidative

https://doi.org/10.5194/egusphere-2026-2161
Preprint. Discussion started: 23 April 2026

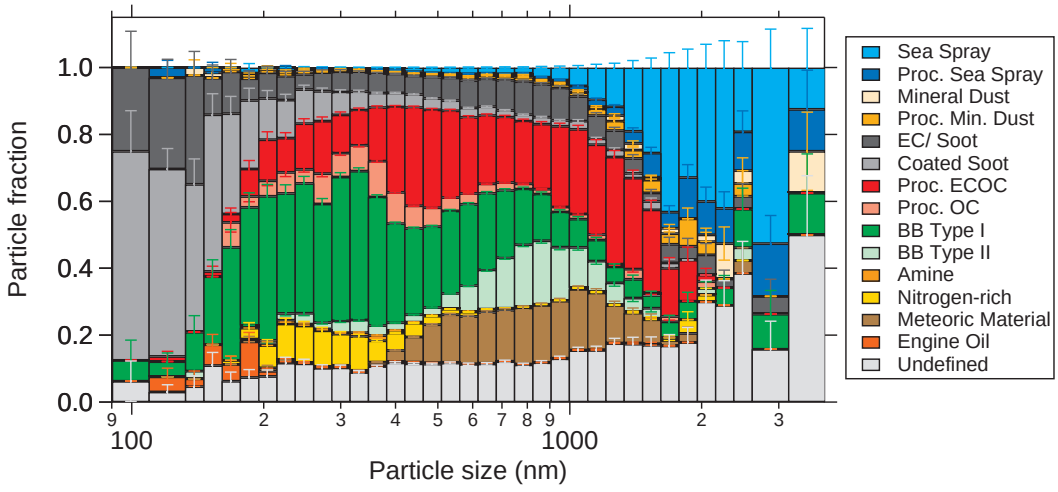

Figure 4. Size distribution of the particle types detected with the ERICA-LAMS at the scoop aerosol sampling system. The error bars illustrate the uncertainty of the particle fraction as a result of the binomial counting statistics (Sect. S7).

aging, both BB types revealed similar results for the fraction of organic ion signals at $m/z + 43$ (f43) and $+44$ (f44) of the total organic mass obtained by the ERICA-AMS which can be used as a proxy for oxidative aging of organic aerosol (Ng et al., 2010, 2011). BB Type I revealed an age of few weeks whereas BB Type II remained in the atmosphere for some months. The age and potential source regions will be discussed in Sect. 3.1. A detailed analysis of the oxidative aging is provided in Sect. S4.2.

UTLS aerosol over Germany affected by long-range transport

The carbonaceous aerosol in the wintertime UTLS over Germany is controlled by long-range transport of BB aerosol from North America. Backward air mass trajectories derived from the Hybrid Single-Particle Lagrangian Integrated Trajectory Model (HYSPLIT, Sect. S4) indicate the transport of air masses from the Pacific US coast to the air space area probed in North Germany. Figure 6 provides an overview of the backward trajectories for RF3 which revealed the largest contribution of air masses originating from the Pacific US Coast along with the largest particle fraction of BB Type I (Fig. 7a). The trajectories partly originate from the East Pacific or reach a low level next to the Pacific US coast (red box in Fig. 6) that was affected by the Thomas Fire (red cross in Fig. 6), a massive wildfire taking place in December 2017 and January 2018. In total, the US National Fire Interagency Fire Center reported 3257 wildfires burning 71,189 acres (≈ 288.1 km^2) in January 2018 within the United States (NOAA-NCEI, 2018), the second largest number of fires in January since 2000 (largest number of 3507 in 2006 burning 330,447 acres ≈ 1337.3 km^2). We have indications that the occurrence of BB Type I is connected to the impact of air masses of North American origin. As Figure 7a reveals, the PF of BB Type I is increasing with the number of trajectories approaching from the Pacific US coast and contributing to the air mass probed along the flight tracks in North Germany is

https://doi.org/10.5194/egusphere-2026-2161
Preprint. Discussion started: 23 April 2026

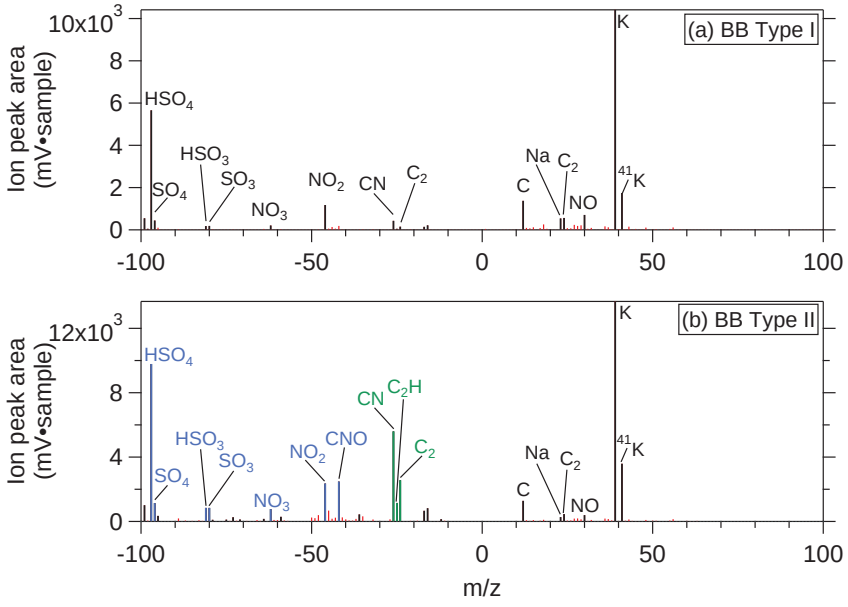

Figure 5. Mean bipolar mass spectrum of BB Type I (a) and BB Type II (b) detected during ND-MAX. The black sticks display the characteristical ion marker peaks, the blue sticks the additional signature of nitrate and sulfate material included in BB Type II particles versus BB Type I. Green sticks mark the enhanced organic material in BB Type II. Red sticks refer to minor signals that were disregarded for the determination of the particle types. The mean mass spectrum includes ERICA-LAMS data of RF1–RF6 and RF8.

increased. We thus conclude the particles of BB Type I to be transported across the Atlantic Ocean within the troposphere within days to weeks. In contrast, BB Type II cannot be directly assigned to wildfires located at the Pacific US coast (Fig. 7b). Further, we analyzed three air mass samples of different air mass origin, and observed a variable occurrence of the two BB types. Figure 8 shows the particle fraction of both BB types considering three individual air mass samples. BB Type I is predominant in air masses of subtropic origin, whereas BB Type II dominates biomass burning material in air masses traced back to polar regions. The particle fraction of BB Type II is decreasing as less air mass trajectories are traced back to polar regions. In contrast, BB Type I is the only type detected when the trajectories reach back to subtropic regions below 30° N. Since BB Type II appears more frequently in polar regions, which do not provide appropriate conditions for wildfires in the winter season, these particles must have been injected to the stratosphere before, and were potentially distributed in the polar region as part of the subsiding branch of the BDC.

Indeed, we measured enhanced mass concentrations of organic material along with increased particle fractions of biomass burning and EC/soot particles, respectively, in air masses with stratospheric signature (Fig. 2a). Figure 9 provides a comparison of three-dimensional profiles of the organics mass concentration obtained with the ERICA-AMS and of particle fractions of

https://doi.org/10.5194/egusphere-2026-2161
Preprint. Discussion started: 23 April 2026

BB Type II along with EC/soot recorded with the ERICA-LAMS. Additionally, isolines of potential vorticity (PV) highlight the regions of stratospheric signature (equivalent latitude and potential vorticity were taken from the ERA5 dataset, Hersbach et al., 2018, 2020). The profiles display an enhanced organic mass concentration and particle fraction of biomass burning and soot particles towards larger altitude and equivalent latitude levels. Local maxima in the mass concentration and particle fraction are observed in regions of a potential vorticity larger than 2 PVU, implying a stratospheric signature. Due to the enhancement of both, the organic material and the biomass burning particle type along with EC/soot particles, we assume this particle loading to be of wildfire origin. Indeed, Baars et al. (2019) and Bourassa et al. (2019) reported a record-breaking forest fire activity in British Columbia during August 2017 that probably could have affected the particle concentrations detected during ND-MAX. The "Pacific Northwest Event" (PNE) describes a series of wildfires triggering five massive thunderstorms (so-called pyrocumulonimbus, pyroCb) that injected large amounts of smoke particles of biomass burning origin into the lower stratosphere. Subsequently, the particles were transported downwind along the jet stream reaching Europe within a week and circulated around the Northern Hemisphere for several weeks (Khaykin et al., 2018; Peterson et al., 2018). Satellite retrieval data such as stratospheric aerosol optical thickness and particle extinction coefficients indicated an enhancement in aerosol loading up to April 2018 (Baars et al., 2019; Yu et al., 2019). Thus, we assume the detected enhancement of organic aerosol and especially of both particle types, BB Type II and EC/soot, within air masses of stratospheric influence to be related to these intensive wildfires. However, organic aerosol of the PNE was also transported around the eastern flank of the Asian Monsoon Anticyclone into the tropics where it was lifted upwards as part of the BDC, also indicating a potential source and transport path for the organic material (Kloss et al., 2019; Martinsson et al., 2019). Further processes such as local intrusion or mixing across the tropopause may also contribute to organic material in general (Gettelman et al., 2011), but the enhancement of organic material in the LMS agrees with the enhancement of aerosol optical thickness presented by Baars et al. (2019) and Yu et al. (2019).

In conclusion, we detected two BB types in the wintertime UTLS region over Germany as a result of long-range transport processes. BB Type I is traced back to the Thomas Fire located at the Pacific US coast and is expected to have an age of days to weeks. In contrast, BB Type II is mostly present in air masses of stratospheric signature and air masses traced back to polar regions which are potentially affected by a BB plume resulting from the PNE and, thus, suggesting an age up to 6 months. The particle size also implies BB Type II to be shifted to larger particle diameters and thus more chemically aged compared to BB Type I. The chemical composition of both BB types is partly in line: the mass spectrum of BB Type II contains more signatures of secondary material such as nitrate and sulfate, implying a further aging compared to BB Type I.

Aerosol chemical composition influenced by local meteorological conditions

Although the long-range transport of BB particles is an important source for UTLS particles, the local meteorological conditions have also a significant effect on the composition of the aerosol particles. The local tropopause level shifts the abundance of particles containing meteoric material and the gradient of sulfate aerosol along the tropopause layer. The particle fraction of meteoric material starts to increase at 7 km during the cold period from 4 % up to 49 % at 11.5 km (Fig. 2a). Within the warm period, the occurrence of meteoric material is mostly shifted to higher altitude levels not covered by the RFs, consistent

https://doi.org/10.5194/egusphere-2026-2161
Preprint. Discussion started: 23 April 2026

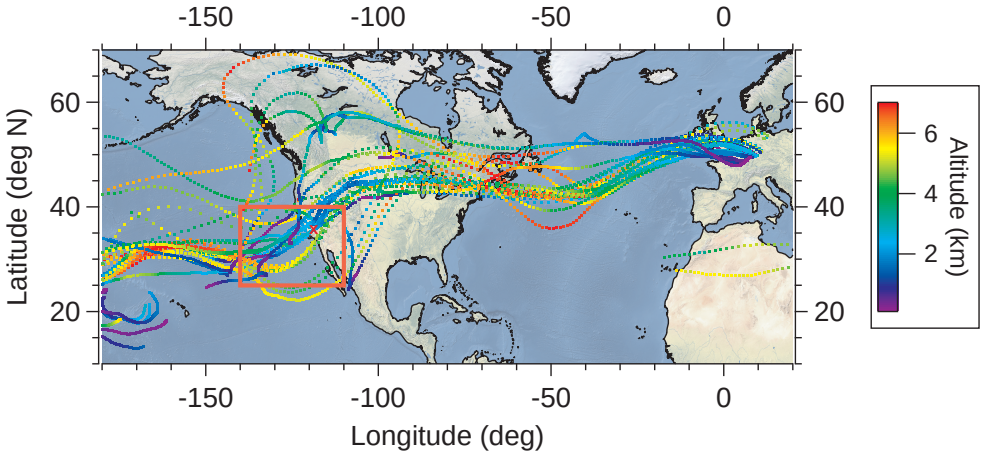

Figure 6. Selection of backward trajectories simulated for RF3 from 23 January 2018. Trajectories were started from the aircraft position, traced back up to 10 days, and filtered for those affected by the Pacific US coast BL (red box) along with wildfires (indicated by the red cross), color-coded with the altitude as an indicator for the potential source region. The map was created with data from Kelso and Patterson (2025).

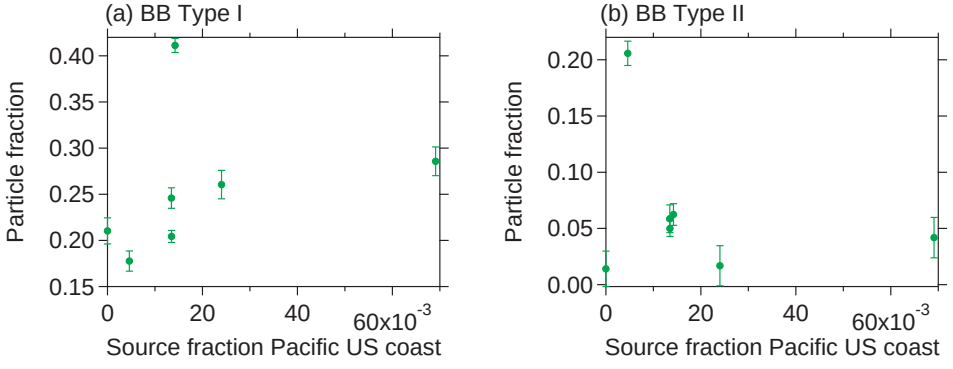

Figure 7. Abundance of BB Type I (a) and BB Type II (b) for a variable contribution of Pacific US coast as source region. The error bars illustrate the uncertainty of the particle fraction as a result of the binomial counting statistics (Sect. S7).

with the tropopause transition layer. An enhancement in the particle fraction is observed for altitude levels above 10 km (Fig 2b). The sulfate profile obtained by the ERICA-AMS is also affected by a shift of the tropopause level. The strong gradient of sulfate mass concentration, observed between 6 and 9 km during the cold period (Fig. 3a), is not observed during the warm period. However, the sulfate profile indicates a gradient for altitude levels above 11 km (Fig. 3b).

The wind circulation has impact on the occurrence of sea spray aerosol. The vertical profile (Fig. 2a) reveals a distinctive abundance of sea spray up to 50 % below 4.5 km which is in contrast to the low particle fraction of sea spray detected during

https://doi.org/10.5194/egusphere-2026-2161
Preprint. Discussion started: 23 April 2026

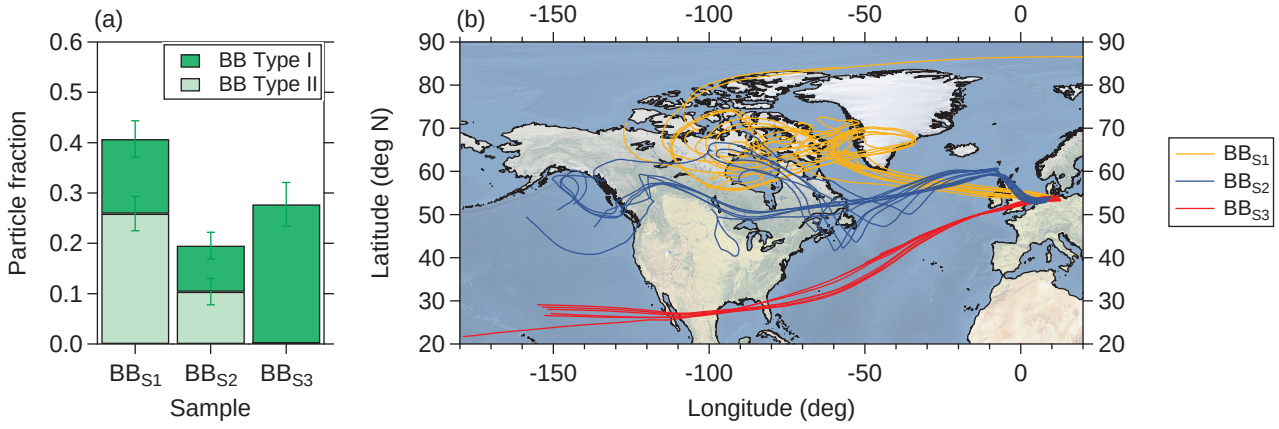

Figure 8. Relative abundance of BB particles for three selected air mass samples (a): BB_{S1} — RF1, 13:05:00–13:17:46, BB_{S2} — RF8, 10:38:00–10:49:51, and BB_{S3} — RF5, 13:25:00–13:37:39. The particle fraction refers to the entirety of the particles measured within the sample periods. The error bars illustrate the uncertainty of the particle fraction as a result of the binomial counting statistics (Sect. S7). HYSPLIT backward air mass trajectories for the periods of the three air mass samples (b), color-coded by the corresponding sample. The map was created with data from Natural Earth.

the warm period. Figure 10 provides an overview of the high-level temperature fields as well as dynamics (isohypses at 850-hPa-level), and pressure pattern at mean sea level pressure (isobars) that were frequently observed during ND-MAX and are assigned to the cold period. The measurement region is affected by a northwestern circulation, indicated by the ensemble of isobars that separate the low-pressure system over Northern and Eastern Europe from an anticyclone located over the Atlantic Ocean. A more detailed analysis of the meteorological conditions is provided in Sect. S5.1. The northwestern winds lead to an enhancement in the detected sea spray fraction, probably by the advection of marine air masses from the North Sea and Norwegian Sea.

3.2 Carbonaceous aerosol in the wintertime UTLS also driven by aircraft exhaust

The sampling of aircraft exhaust was one of the primary goals of the ND-MAX campaign. Here, we present the particle types that were attributed to the aging of an exhaust plume and the difficulty in the analysis of the particle chemical composition. The relative occurrence of the individual particle types was determined for variable distances of the DLR-ATRA and the following NASA DC-8 aircraft in order to attribute these types to potential aircraft emissions. We have evidence that EC/soot, coated soot, and engine oil contribute to the chemical composition of exhaust plumes. Figure 11 displays the relative occurrence of these particle types as a function of the aircraft distance, divided into bins of 2 km. The distance analysis reveals that the abundance of the particle types is increasing with decreasing distance between the NASA DC-8 aircraft and the DLR-ATRA flying ahead. For each particle type, the maximum is detected in a distance of 5 km behind the DLR-ATRA and at a median plume age of approximately 30 s, in agreement with the maximum of the CO_2 volume mixing ratio of 412.4 ppmv. The larger

https://doi.org/10.5194/egusphere-2026-2161
Preprint. Discussion started: 23 April 2026

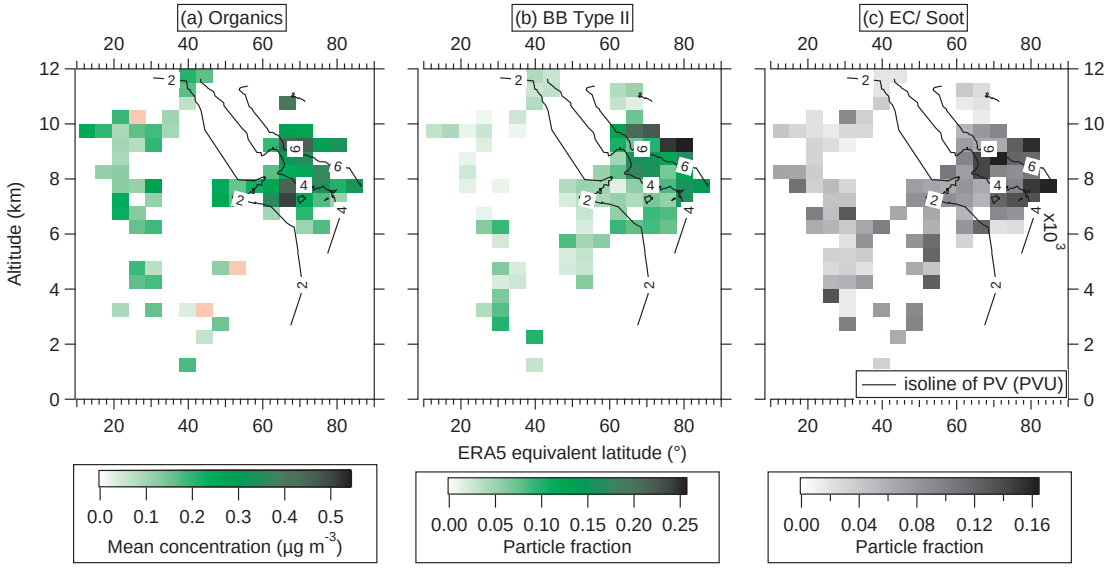

Figure 9. Spatially and vertically resolved aerosol composition during ND-MAX. ERICA-AMS mass concentration of organics (green) (a), particle fractions detected with the ERICA-LAMS of BB Type II (green), and EC/soot (gray). Colors show mean concentration (a) and particle fraction (b and c) for each grid cell of 4.5° in equivalent latitude and 500 m in altitude. The black lines represent the 2,4,6 and 8 PVU isolines in the corresponding equivalent latitude bin. AMS-Data include RF1–RF5 and RF8, LAMS-Data include RF1–RF6 and RF8. Red-colored bins refer to negative mass concentrations.

the distance between the two aircraft, the lower is the relative abundance of the assigned particle types and the CO_2 mixing ratio, implying the entrainment of ambient air into the exhaust plume. We thus conclude that these particle types are emitted by the aircraft turbines as small particles with subsequent growth of the particles in the ERICA detectable size range. Besides their potential biomass burning origin, EC/soot particles are well-known pollutants released during the aircraft (engine) combustion process (Yu et al., 2024; Voigt et al., 2021; Onasch et al., 2009). However, engine lubrication oil has raised recent attention as this substance appears frequently in the presence of aircraft exhaust (Ungeheuer et al., 2022; Yu et al., 2012) and their chemical composition is comparable to those of laboratory measurements of reference engine oils (Clemen et al., in prep.). Further, all three types were observed in the size range below 150 nm (Fig. 4), indicating these particle types as of engine origin. Yu et al. (2024) reported soot emissions with a median diameter of 35 nm and Schripp et al. (2018) showed particle size distributions of particulate emissions from the DLR-ATRA, primarily identified as non-volatile black carbon, ranging between 10 and 50 nm.

However, we could not identify fresh aircraft emissions using ERICA-LAMS due to particle diameters below the lower detection limit. Soot and small volatile particles were measured in the exhaust plume of the aircraft engines of the DLR-ATRA with other instruments (Schripp et al., 2022; Voigt et al., 2021; Bräuer et al., 2021a). Regarding ERICA-LAMS, Hünig (2020) reported a lower detection limit of approximately 170 nm (with 50% detection efficiency, d_{50}). In accordance with this, during ND-MAX we mostly measured particles with vacuum-aerodynamic diameters between 200 and 2000 nm (Fig. 12), a size range well beyond the typical sizes of freshly emitted particles from fuel combustion. In consequence, fresh exhaust-related

https://doi.org/10.5194/egusphere-2026-2161
Preprint. Discussion started: 23 April 2026

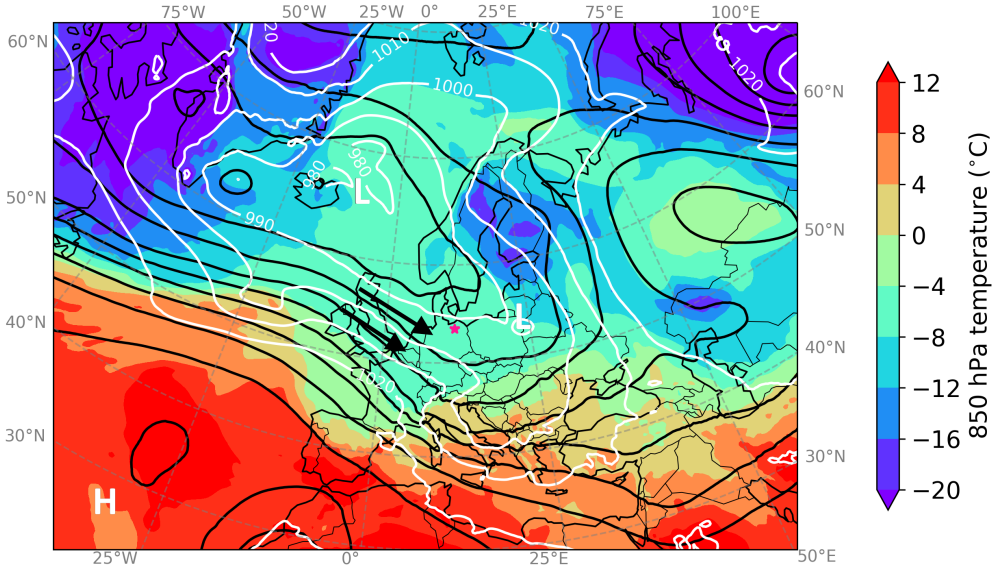

Figure 10. Weather map of 17 January 2018, 12:00 UTC including isohypses at 500-hPa-level (black lines) and mean sea level pressure (white lines), 'H' and 'L' mark the center of high-pressure and low-pressure systems, respectively. The black arrows denote the wind circulation. The color-coding refers to ambient temperatures at the 850-hPa-level and denotes the distribution of warm and cold air masses. The pink star denotes the measurement area of RF1. ERA5 data were provided by Hersbach et al. (2018).

aerosol particles of diameters below 200 nm are underrrepresented in the aerosol population detected by ERICA-LAMS and, thus, hardly allow for a differentiation between air masses of atmospheric background and of exhaust plumes. Figure 13a provides an overview of the particle fractions obtained with the ERICA-LAMS in periods of aircraft exhaust and atmospheric background. Comparing the chemical composition of both, aircraft exhaust and background air masses (outside clouds), in the size range of ERICA-LAMS, the relative abundance of individual particle types is very similar for both periods. For instance, processed ECOC particles are found in 22.7 % (20.8 %) of all particles detected within the exhaust (background) period, processed OC particles in 3.2 % (3.9 %). Major differences are observed for the meteoric material (10.5 %) which is due to larger travel times of the aircraft in the stratosphere. Most of the particles (88.3 %) analyzed during the Exhaust periods were measured in the ExTL and stratosphere, usually accompanied by meteoric material. However, only 71.9 % of the particles measured within the background periods are measured in the ExTL and stratosphere. Thus, the particle fraction of meteoric material coincides with a larger impact of air masses of stratospheric origin.

However, Figure 13b shows the particle composition of exhaust and background air limited to a maximum size of 200 nm. Aerosol particles below 200 nm in size were hardly detected but indicate a signature of fossil fuel combustion in aircraft exhaust plumes. EC/soot and coated soot show enhanced particle fractions (EC/soot: 25 % versus 16 %; coated soot: 56 % versus

https://doi.org/10.5194/egusphere-2026-2161
Preprint. Discussion started: 23 April 2026

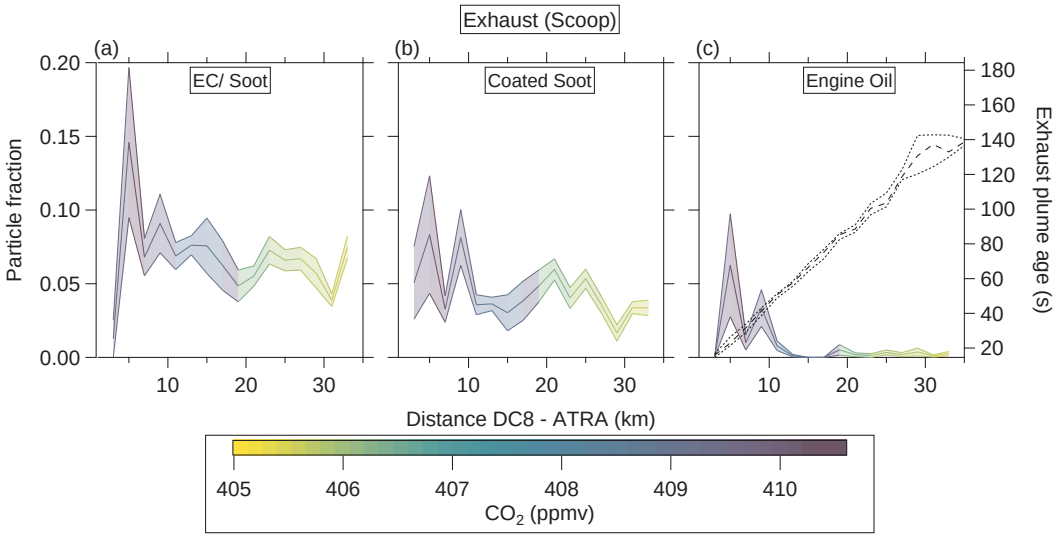

Figure 11. Distribution of the relative abundance of exhaust-related a) EC/soot, b) coated soot, and c) engine oil particles detected by the ERICA-LAMS as a function of distance between the exhaust plume generating DLR-ATRA and the Flying Laboratory NASA DC-8 during ND-MAX, color-coded with measured volume mixing ratio of CO_2. Meausurements consider the exhaust plumes measured with the scoop aerosol inlet. The dashed black line in the right panel reveals the exhaust plume age. The shaded area (dotted lines) illustrates the uncertainty of the particle fraction (plume age) as a result of the binomial counting statistics (Sect. S7).

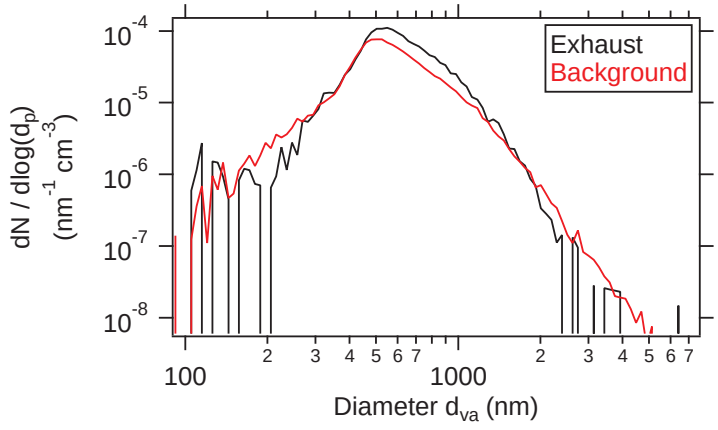

Figure 12. Size distribution of particle number concentration (normalized with respect to the measurement period) detected with the ERICA-LAMS via the scoop inlet during ND-MAX, separated into exhaust (black) and background (red) periods.

23 %) in exhaust plumes compared to ambient aerosols in the atmospheric background (Fig 13b). Although the measurements do not provide a solid statistical foundation for particle sizes below 200 nm in diameter (total counts of 32 in exhaust plumes and of 30 in the atmospheric background, respectively), a positive trend of EC/soot and coated soot particles is observed for

https://doi.org/10.5194/egusphere-2026-2161
Preprint. Discussion started: 23 April 2026

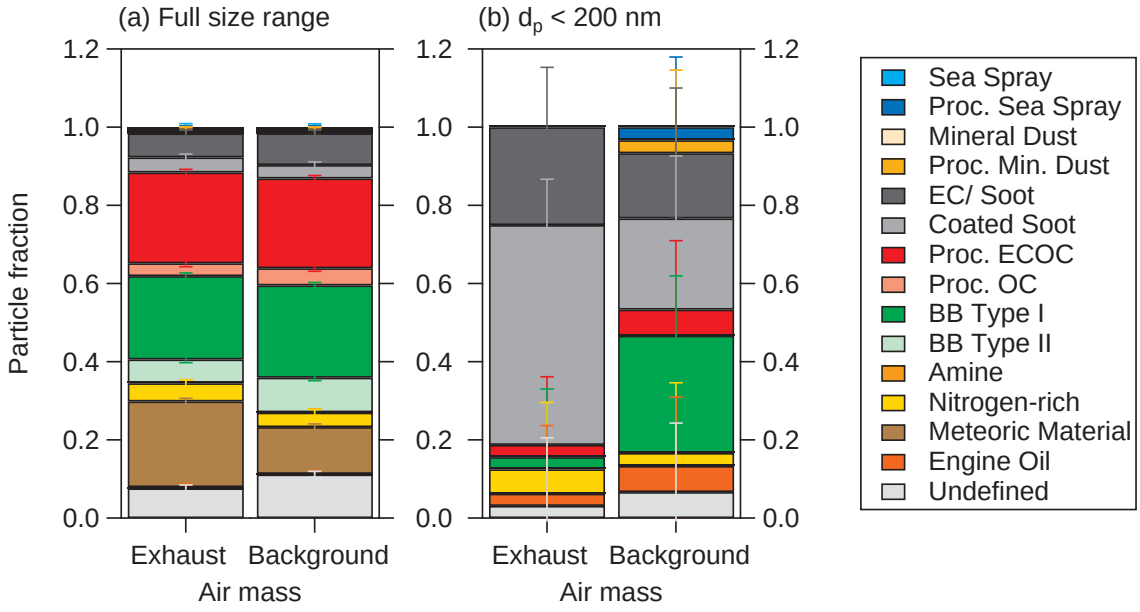

Figure 13. Overview of the relative abundance of detected particle types for exhaust and background periods during the ND-MAX campaign considering the the full size range of ERICA-LAMS (a) and considering particles of sizes below 200 nm (b) in particular. Only measurement periods of RF1–6 and RF8 were considered, that included side-by-side exhaust plumes and background periods in the altitude range of 7.9 to 11.6 km. The error bars illustrate the uncertainty of the particle fraction as a result of the binomial counting statistics (Sect. S7).

exhaust plumes, also confirming these particle types as exhaust-related.

In conclusion, we could show that EC/soot, coated soot, and engine oil are attributed to aircraft exhaust. Thus, emissions of aircraft engines also contribute to the aerosol population and, potentially, participate in chemical processes taking place in the UTLS. As these particle types were measured in the lowermost size bins of ERICA, affected by the detection limit of the ERICA-LAMS, the number of exhaust-related particles is expected to be larger than the concentration obtained during the campaign.

3.3 The chemical signature of cloud residuals in the UTLS

Chemical composition of cloud particle residuals

In addition to aerosol measurements using the scoop inlet in periods under cloud-free conditions, the CVI was used to sample CPRs inside clouds. In a first step, we analyzed the difference between cloud-free aerosols and the CPRs measured with the CVI. For this, all CVI-measurements were combined, which can include ice particle as well as mixed phase cloud residuals. The CPRs detected by the CVI show significant differences from the composition of ambient aerosol (Fig. 14a). Refractory material such as sea spray and mineral dust make up to 50 % of all CPRs detected during ND-MAX, emphasizing the impor-

https://doi.org/10.5194/egusphere-2026-2161
Preprint. Discussion started: 23 April 2026

tance for cloud formation. Furthermore, particles of biomass burning origin provide the largest fraction within organic material in CPRs. This can indicate a high nucleation ability of the BB material. Obviously, the biomass burning particles were well-distributed in the upper troposphere and tropopause region over Germany and also participated in cloud processing. We have evidence, that BB Type I contains smaller signals of secondary material such as nitrate and sulfate (Sect. 3.1). In consequence, this particle type might contain less particle coating and, thus, less concealing of the ice-active sites, resulting in a larger ice nucleability (Fig. 14a; Jahl et al., 2021). 21.5 % are attributed to BB, followed by a fraction of 5.8 % to fresh and coated soot residuals, and 5.2 % of processed ECOC. Fresh and coated soot can act as ice-nucleating particles as shown by Mahrt et al. (2018, 2020). Minor contributions are observed from amines (0.6 %) and processed OC (0.2 %). Residuals of engine oil are found in 4.4 % of all CPRs.

Cirrus residuals

In a second step we focused on ice cloud such as cirrus and contrail residuals according to Sect. 2.4 and S3. Refractory material dominates cirrus residuals detected in the winter upper troposphere over Germany. Figure 14b reveals an overview of the relative abundance of particle types obtained in the ice residuals detected with the CVI in cirrus clouds and contrails. More than 50 % of all cirrus residuals were attributed to sea spray (41.8 %) or processed sea spray (10.5 %), followed by mineral dust in its less processed (8.1 %) and more processed (12.8 %) form. Sea spray is well-known for its large nucleability as a CCN (O'Dowd et al., 1997; Pierce and Adams, 2006; Andreae and Rosenfeld, 2008), and thus, a suitable indicator for liquid-origin cirrus (Luebke et al., 2016). In contrast, mineral dust is rather known for its high activity as INP (Richardson et al., 2007; Hoose et al., 2008; Barahona et al., 2010). However, the presence of soluble material such as sodium chloride or sulfuric acid may enhance the fraction of mineral dust that acts as a CCN by creating a soluble and hygroscopic particle coating (Levin et al., 2005; Kelly et al., 2007; Karydis et al., 2011). Additionally, the processing can reduce the potential for ice formation (Archuleta et al., 2005). As a consequence, the low fraction of pure mineral dust along with the enhanced fraction of processed mineral dust imply the formation of the probed cirrus clouds based on CCN with subsequent freezing.

The meteorological background provides favorable conditions for cirrus formation such as water vapor saturation with respect to ice during RF5. However, cirrus residuals were also detected under sub-saturated conditions ($RH_{Ice} > 80\%$) during RF6. Figure 15 shows an overview of the cirrus and contrail particle residuals detected under variable relative humidities with respect to ice. Cirrus residuals were predominantly detected within 80 and 120 % RH_{Ice}. All cirrus residuals of RF5 were detected in the vicinity of water vapor (super)saturation with respect to ice ($RH_{Ice} \geq 100\%$) that is confirmed by the simulation of backward air mass trajectories (Fig. 16). On average, the resulting trajectories reveal the transport of water vapor to the upper troposphere as part of a WCB, providing a warmed and well-humidified ($RH_{ice} > 100\%$) environment for the formation of cirrus clouds in an altitude range of 5 to 8 km. In contrast, the cirrus residuals of RF6 were measured under sub-saturation with respect to ice which might be the consequence of air mass subsidence. Indeed, the air mass trajectories of RF6 remained on a constant altitude level and revealed a relative humidity with respect to ice in the range from 30 to 60 % (Fig. 16).

https://doi.org/10.5194/egusphere-2026-2161
Preprint. Discussion started: 23 April 2026

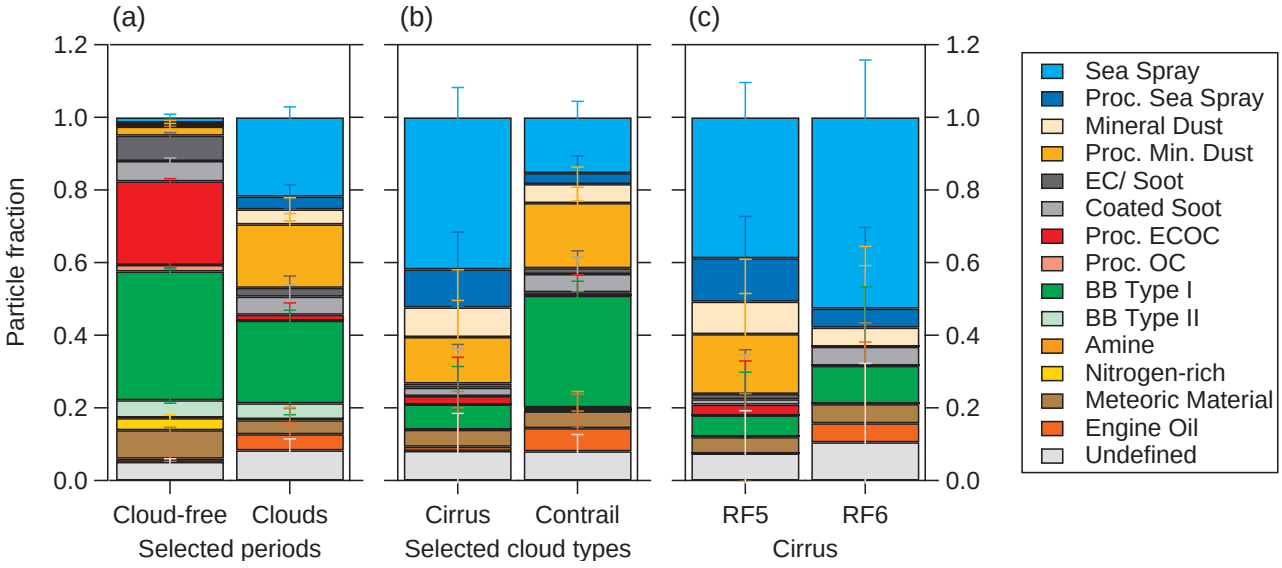

Figure 14. Overview of the relative abundance of sampled particle types in selected periods (a, outside clouds by the scoop inlet and of all cloud residual types (incl. ice and mixed-phase clouds) sampled at the CVI inlet), for selected cloud types (b, Cirrus and Contrails sampled at the CVI), and for Cirrus of RF5 and RF6 in particular (c). For the purpose of comparison, only measurement data of RF5 and RF6 are considered since they provided both, cirrus and contrail data. The error bars illustrate the uncertainty of the particle fraction as a result of the binomial counting statistics (Sect. S7).

Figure 14c compared the composition between cirrus induced by WCB (RF5) and cirrus formed under variable meteorological conditions (RF6). WCB-induced cirrus (of RF5) are dominated by refractory material, mainly differing from other cirrus of RF6 by the presence of processed mineral dust. Almost 80 % of the cirrus residuals sampled during RF5 are attributed to sea spray and mineral dust (Fig. 14c), either to the less or more processed type, indicating the large impact of these particle types on the cirrus formation process. Especially, processed mineral dust is only detected within cirrus clouds induced by the WCB, implying that this particle type has been uplifted by the WCB, providing an additional source of refractory material to the UTLS. Sea spray, processed sea spray, and mineral dust were also detected in cirrus clouds not immediately affected by WCBs (during RF6), implying these particle types to be participating in the cirrus formation process. Further, the measurements suggest that cirrus formation based on refractory material such as sea spray and mineral dust is the preferred process, especially when this material is largely abundant. However, also organic material can contribute to cirrus residuals and is more frequently sampled when refractory material in the UTLS region is limited. Nevertheless, the statistical foundation of cirrus data from RF5 and RF6 is poor as 67 (19) data points were obtained for RF5 (RF6), respectively. In consequence, the findings need to be confirmed by additional measurements.

https://doi.org/10.5194/egusphere-2026-2161
Preprint. Discussion started: 23 April 2026

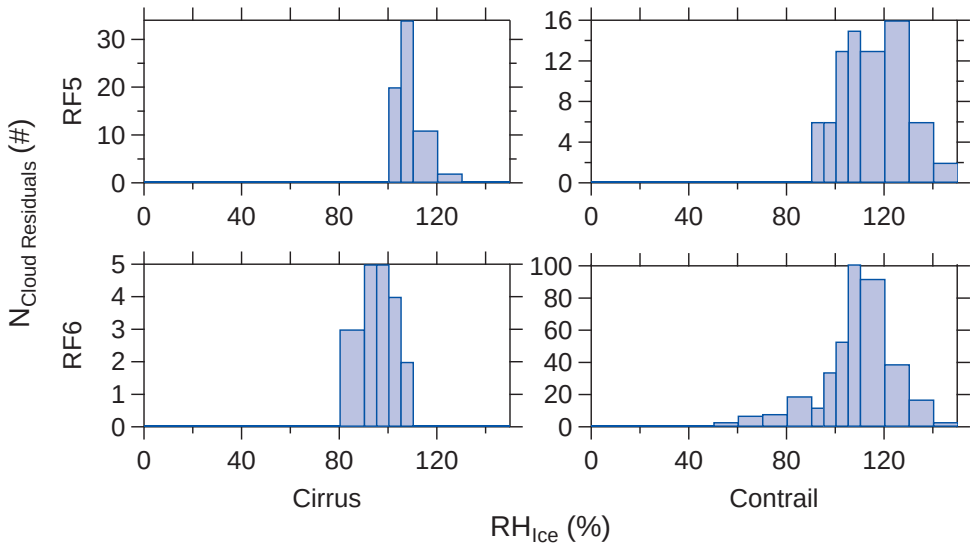

Figure 15. Distribution of the cirrus and contrail particle residuals for relative humidity with respect to ice (RH_{Ice}).

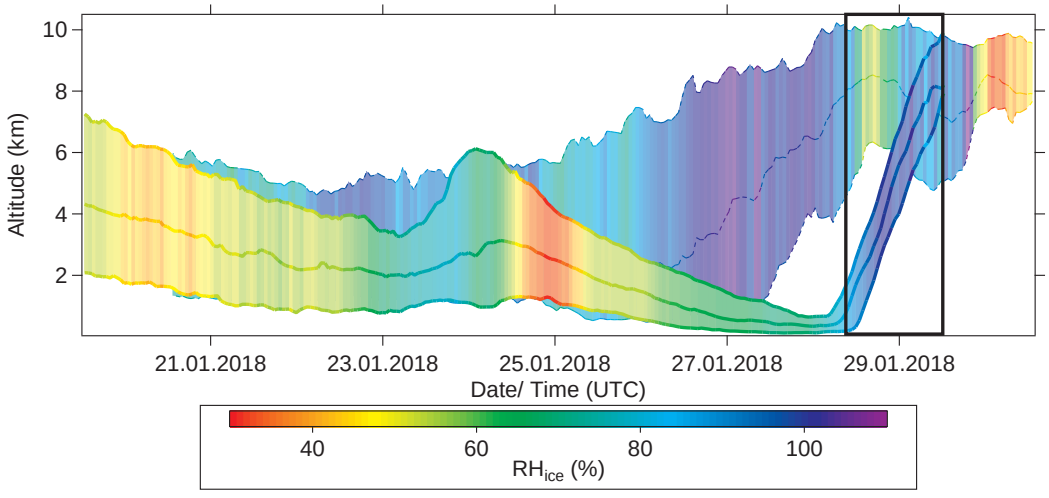

Figure 16. Vertical cross section of the median, 25th and 75th percentile of backward trajectories simulated with HYSPLIT for RF5 (thick, solid lines) and RF6 (thin, dashed lines), color-coded with the median of relative humidity (RH_{ice}). A strong ascent of the median of trajectories is displayed for RF5 on 29 January 2018, indicating an uplift of well-humidified ($RH_{ice} >\sim 100$ %) air masses by a WCB connected to a low pressure system. The black box marks the ascent period. In contrast, the trajectories of RF6 only mark small fluctuations in altitude between 29 and 30 January 2018, along with unsaturated air masses.

https://doi.org/10.5194/egusphere-2026-2161
Preprint. Discussion started: 23 April 2026

Contrail residuals and aircraft signature

Besides aerosol particles of natural origin, the contrail residuals reveal a clear chemical signature of aircraft emissions (Fig. 14b). Similar to the cirrus residuals, refractory material contributes significantly to the contrail residuals with sea spray, processed sea spray, mineral dust, processed mineral dust, and meteoric material. In addition, biomass burning particles (BB Type I) are frequently found in contrail residuals. However, a comparison of sample periods attributed to atmospheric background and to aircraft exhaust plumes suggest that the presence of BB Type I is driven by the atmospheric background (Fig. S14). In addition to particle types of natural origin, aircraft-related types are found in 13.1 % of the detected contrail residuals. Despite the small fraction, their enhancement in relative abundance compared to cirrus residuals is clearly visible. In detail, engine oil and coated soot are more frequently detected in contrails (6.4 % and 5.0 %) than in cirrus events (1.2 % and 2.3 %), implying the anthropogenic types to contribute to contrail formation. The overall low contribution of exhaust-related particles might be the consequence of dilution: The majority of contrail residuals (144 in 177) is sampled in contrail events older than 60 s, corresponding to a dilution ratio of $1.85 \cdot 10^5$ when applying the formula as mentioned in Schumann et al. (1998). Thus, the aircraft exhaust plume is diluted by the entrainment of ambient air, reducing the relative occurrence of combustion byproducts. Also, the exhaust-related particle residuals might be too small after evaporation of the ice crystals, not allowing for a detection with the ERICA-LAMS. In conclusion, contrail residuals observed during ND-MAX contain a clear chemical signature of aircraft emissions besides natural constituents. However, the lower detection limit of the ERICA-LAMS might oversee small-sized contrail residuals, affecting the aircraft footprint inside upper tropospheric clouds.

4 Conclusions

The aerosol chemical composition of the wintertime UTLS region over Germany was analyzed by obtaining the ERICA aerosol mass spectrometer. The ERICA measurements include qualitative single-particle measurements with the ERICA-LAMS and quantitative particle ensemble measurements based on the ERICA-AMS. Carbonaceous material dominates the particulate matter in the wintertime upper troposphere and tropopause region over Germany. About 80 % of all particles detected by the ERICA-LAMS are attributed to carbonaceous compounds, among which biomass burning material is the dominating species. The further into the LMS, the higher becomes the fraction of meteoric and sulfate material.

We obtained two different types of BB particles, differing in their particle size range, occurrence, and chemical signature. Particles of BB Type I were majorly detected up to 800 nm and were sampled from the ground to the LMS. In contrast, BB Type II ranged between 500 and 1500 nm and was mainly detected in lower stratospheric air masses, there being more frequently detected along with soot particles. Further, we have evidence that BB Type II contains more secondary material such as nitrate and sulfate, implying a higher degree of aerosol processing. As BB Type II is mainly detected in the LMS which is accompanied by sulfuric acid, this type is expected to undergo a longer aging process than BB Type I. However, BB Type II includes more organic material than BB Type I that is unexpected and emphasizes the need for further investigation of the aging process in the UTLS.

https://doi.org/10.5194/egusphere-2026-2161
Preprint. Discussion started: 23 April 2026

Long-range transport of BB aerosol from North America controls the carbonaceous aerosol in the wintertime UTLS over Germany. Backward air mass trajectories of HYSPLIT suggest the BB Type I to result from the Thomas Fire taking place at the Pacific US Coast. The particle fraction rises when the contribution of this source region is enhanced. Further, we measured an enhancement in the organic mass concentration by the ERICA-AMS along with enhanced particle fractions of BB material and EC/soot obtained with the ERICA-LAMS in air masses containing a stratospheric signature. We assume this material to originate from the "Pacific Northwest Event" as this series of wildfires triggered pyro-convection, leading to a transport of the wildfire plumes into the lower stratosphere and subsequent distribution along the Northern Hemisphere with signatures detectable until April 2018 (Baars et al., 2019; Yu et al., 2019).

We have evidence that the aerosol chemical composition is additionally controlled by local meteorological conditions. The local tropopause is shifted as a consequence of ascending and descending air masses, also resulting in a shift of the abundance of meteoric or sulfate material. The wind circulation has impact on the presence of sea spray aerosol that is mainly enhanced under the influence of northwestern winds advecting air masses from the North Sea and Norwegian Sea.

We showed that EC/soot, coated soot, and engine oil in the UTLS region can be partly attributed to aircraft emissions. The occurrence of these particle types decreases with increasing aircraft distance between the NASA DC-8 and the DLR-ATRA flying ahead. The majority of these particles reveals sizes (in vacuum-aerodynamic diameter) below 200 nm and is, thus, underrepresented in the aerosol population detected by ERICA-LAMS. Hence, we expect the particles of EC/soot, coated soot, and engine oil to just have grown to sizes being detectable by ERICA-LAMS and the majority of fresh aircraft emissions to be too small for a detection with ERICA-LAMS. In contrast, large-sized aerosol particles above 200 nm mainly consisted of particles types that were present in both, the atmospheric background and exhaust plumes, implying aircraft exhaust to mainly contribute to small-sized aerosol particles.

Beside aircraft emissions, we investigated the chemical composition of cirrus clouds and contrails in the wintertime UTLS over Germany by sampling through a CVI. Our results show that almost 50 % of the CPRs detected during RF5 and RF6 are assigned to refractory material, emphasizing their importance for cloud formation. Within carbonaceous matter in CPRs, BB material provides the largest fraction, implying its high nucleability and large abundance in the upper troposphere and tropopause region. However, BB Type I is the only relevant type within cirrus and contrail residuals due to its large abundance compared to BB Type II. Regarding cirrus, almost three quarters of CPRs are assigned to sea spray and processed mineral dust that imply the cirrus formation at a liquid stage, also indicated by the WCB during RF5. Processed mineral dust was only detected within cirrus residuals of RF5, implying this particle type to be uplifted by the WCB. A comparison of cirrus induced by WCB and of cirrus of variable meteorological conditions revealed that the formation process via refractory material is the preferred way. However, this needs to be confirmed by additional measurements.

Considering the composition of contrails older than 60 s, the residuals consist of refractory and carbonaceous material. Aircraft-related types such as engine oil and coated soot lead to an anthropogenic chemical signature of contrails and are in line with the enhancement of these compounds found in aircraft exhaust plumes. We assume this low contribution to be the consequence of dilution effects which reduce the relative occurrence of combustion byproducts. Further, we expect contrail residuals of aircraft exhaust origin to be mainly too small for the detection with ERICA-LAMS. However, this needs to be clearified by

https://doi.org/10.5194/egusphere-2026-2161
Preprint. Discussion started: 23 April 2026

measurements.

This study highlights the large contribution of BB material to the wintertime UTLS aerosol chemical composition in Central Europe, potentially affecting the UTLS radiative forcing. Besides particles containing sulfuric and meteoric substances, organic material may have significant impact on the lowermost stratospheric air masses, thereby contributing to the stratospheric chemistry. Further, we have to reconsider the UTLS chemistry that is not only depending on regular and recurring local processes, but also includes chemical compounds released many thousand kilometers away and transported towards the UTLS region.

Aircraft emissions contribute to the UTLS aerosol population, mainly by the release of EC/soot that can undergo processing, and by engine oil that is predominantly contained in the cloud residuals. Obviously, the exhaust-related particles contribute to the contrail formation, thereby affecting the physico-chemical properties and the radiative forcing of contrails. However, the number of exhaust-related aerosol particles and cloud residuals is underrepresented as their particle size is mainly below the detection limit of the ERICA-LAMS ($\sim 170\ \mathrm{nm}$). A coverage of particle sizes below $100\ \mathrm{nm}$ would help to detect combustion byproducts and potentially allow for the assessment of aircraft exhaust impact on the atmospheric aerosol population and the contrail chemical composition in particular. Limited counting statistics impeded the analysis of cloud residuals sampled with the CVI. Upcoming aircraft experiments in the UTLS region need to enlarge the sample periods of cirrus and contrail events to provide a solid statistical foundation. A larger number of cloud residuals increase the chance to discover more potential cloud or ice nuclei. More measurements are needed to resolve the fraction of aircraft-related particulate matter involved in the nucleation process of contrail droplets. Especially, we need to differentiate between various contrail stages and focus on freshly generated contrails of ages not older than $10\ \mathrm{s}$ when particles activate into water droplets (Kärcher, 2018).

Data availability. The ND-MAX data are available at https://science-data.larc.nasa.gov/aero-fp/projects/. ERICA-data will be included in the course of the review process.

Author contributions. PB performed the analysis of the ERICA-LAMS and ERICA-AMS datasets and generated the corresponding figures. Instrument development and operation during ND-MAX was done by AD, SM, OA, AH, and SB. ERICA-AMS data were processed by OA. OE provided the HYSPLIT output and supported the creation of the high-level weather maps based on ERA5-data. HCC gave me valuable advice on the specification and determination of the aircraft-related engine oil aerosol type. HCL computed trace gas data and meteorological parameter based on the CLaMS model, and interpolated along the flight track. KK provided vertical profiles of the C-ToF-AMS. Complementary data of the CPC and FFSSP as well as trace gas records of CO_2 and O_3 were provided by CV and HS, respectively, for the definition of exhaust-related events. IWC data were provided by BA for the characterization of cirrus origin. LAS data were provided by BA. OA, OE, FK, HCC, JS, CV, and SB gave critical input for understanding and interpreting the ERICA-LAMS and ERICA-AMS data. TB and CV provided expertise on cirrus and contrail data. All authors commented on the manuscript.

https://doi.org/10.5194/egusphere-2026-2161
Preprint. Discussion started: 23 April 2026

Competing interests. The corresponding author confirms that there are no competing interests among the authors.

Acknowledgements. This research was supported by the Deutsche Forschungsgemeinschaft (grant nos. SPP HALO 1294, VO 1504/10-1, and TRR 301 – Project-ID 428312742). DLR within the ECLIF (Emissions and Climate Impact of alternative Fuels) project and NASA support was provided by the NASA Aeronautics Advanced Air Transport Technologies Project within the Advanced Air Vehicles Program and the NASA Airborne Science Program within the Earth Science Division. Additional ground testing support was provided by the U.S. FAA Office of Energy and the Environment as well as Transport Canada. The work on ERICA was financed by the European Research Council under the EU's Seventh Framework Program (FP7/2007-2013)/ERC Grant Agreement No.321040 ("EXCATRO") and supported by the Max Planck Society. Further financial support was received from the Max Plank Graduate Center. HCC acknowledges funding by the DFG through the SPP 1294 (HALO) under grant number SCHN 1138/8-1 (project ID: 442647984). OE and FK acknowledge the funding by the Deutsche Forschungsgemeinschaft (DFG, German Research Foundation) – TRR 301 – Project-ID 428312742: "The tropopause region in a changing atmosphere". The authors thank the technical and scientific coordinators Bruce E. Anderson and Timothy Moes and all teams that were engaged in the field experiments. The authors gratefully acknowledge the NOAA Air Resources Laboratory (ARL) for the provision of the HYSPLIT transport and dispersion model and/or READY website (https://www.ready.noaa.gov) used in this publication. The article processing charges for this open-access publication were covered by the Max Planck Society.

https://doi.org/10.5194/egusphere-2026-2161
Preprint. Discussion started: 23 April 2026

References

Abegglen, M., Brem, B., Ellenrieder, M., Durdina, L., Rindlisbacher, T., Wang, J., Lohmann, U., and Sierau, B.: Chemical characterization of freshly emitted particulate matter from aircraft exhaust using single particle mass spectrometry, Atmospheric Environment, 134, 181–197, https://doi.org/10.1016/j.atmosenv.2016.03.051, 2016.

Agrawal, H., Sawant, A. A., Jansen, K., Wayne Miller, J., and Cocker, D. R.: Characterization of chemical and particulate emissions from aircraft engines, Atmospheric Environment, 42, 4380–4392, https://doi.org/10.1016/j.atmosenv.2008.01.069, 2008.

Almeida, O., Souza, P. R., and Erick Cunha: A Numerical Approach for Implementing Air Intakes in a Canard Type Aircraft for Engine Cooling Purposes, Journal of Aerospace Technology and Management, 13, https://doi.org/10.1590/jatm.v13.1192, 2021.

Anderson, B. E., Cofer, W. R., and Winstead, E. L.: Measurements of Aerosol Parameters Aboard the DC-8 during the Transport and Chemical Evolution over the Pacific Mission, on website, https://www-air.larc.nasa.gov/missions/tracep/AndersonInstrumentDescription.htm, 2015.

Anderson, B. E., Moore, R., LeClercq, P., Corbin, J., Crosbie, E., Lobo, P., Miake-Lye, R., Schripp, T., Whitefield, P., Ziemba, L., Shook, M., Diskin, G., DiGangi, J., Nowak, J., Robinson, C., Yu, Z., Wisthaler, A., Borrmann, S., Mollecker, S., Winstead, E., Smallwood, G., Sauer, D., Kaufmann, S., Bräuer, T., Voigt, C., and Schlager, H.: An Overview of the NASA/DLR Multidisciplinary Airborne Experiment (ND-MAX)/Emission and Climate Impact of Alternative Fuel (ECLIF-2) Mission, in preparation, in prep.

Andersson, S. M., Martinsson, B. G., Vernier, J.-P., Friberg, J., Brenninkmeijer, C. A. M., Hermann, M., van Velthoven, P. F. J., and Zahn, A.: Significant radiative impact of volcanic aerosol in the lowermost stratosphere, Nature Communications, 6, https://doi.org/10.1038/ncomms8692, 2015.

Andreae, M. and Rosenfeld, D.: Aerosol–cloud–precipitation interactions. Part 1. The nature and sources of cloud-active aerosols, Earth-Science Reviews, 89, 13–41, https://doi.org/10.1016/j.earscirev.2008.03.001, 2008.

Appel, O., Köllner, F., Dragoneas, A., Hünig, A., Molleker, S., Schlager, H., Mahnke, C., Weigel, R., Port, M., Schulz, C., Drewnick, F., Vogel, B., Stroh, F., and Borrmann, S.: Chemical analysis of the Asian tropopause aerosol layer (ATAL) with emphasis on secondary aerosol particles using aircraft-based in situ aerosol mass spectrometry, Atmospheric Chemistry and Physics, 22, 13 607–13 630, https://doi.org/10.5194/acp-22-13607-2022, 2022.

Aquila, V., Oman, L. D., Stolarski, R., Douglass, A. R., and Newman, P. A.: The Response of Ozone and Nitrogen Dioxide to the Eruption of Mt. Pinatubo at Southern and Northern Midlatitudes, Journal of the Atmospheric Sciences, 70, 894 – 900, https://doi.org/10.1175/JAS-D-12-0143.1, 2013.

Archuleta, C. M., DeMott, P. J., and Kreidenweis, S. M.: Ice nucleation by surrogates for atmospheric mineral dust and mineral dust/sulfate particles at cirrus temperatures, Atmospheric Chemistry and Physics, 5, 2617–2634, https://doi.org/10.5194/acp-5-2617-2005, 2005.

Arias, P., Bellouin, N., Coppola, E., Jones, R., Krinner, G., Marotzke, J., Naik, V., Palmer, M., Plattner, G.-K., Rogelj, J., Rojas, M., Sillmann, J., Storelvmo, T., Thorne, P., Trewin, B., Achuta Rao, K., Adhikary, B., Allan, R., Armour, K., Bala, G., Barimalala, R., Berger, S., Canadell, J., Cassou, C., Cherchi, A., Collins, W., Collins, W., Connors, S., Corti, S., Cruz, F., Dentener, F., Dereczynski, C., Di Luca, A., Diongue Niang, A., Doblas-Reyes, F., Dosio, A., Douville, H., Engelbrecht, F., Eyring, V., Fischer, E., Forster, P., Fox-Kemper, B., Fuglestvedt, J., Fyfe, J., Gillett, N., Goldfarb, L., Gorodetskaya, I., Gutierrez, J., Hamdi, R., Hawkins, E., Hewitt, H., Hope, P., Islam, A., Jones, C., Kaufman, D., Kopp, R., Kosaka, Y., Kossin, J., Krakovska, S., Lee, J.-Y., Li, J., Mauritsen, T., Maycock, T., Meinshausen, M., Min, S.-K., Monteiro, P., Ngo-Duc, T., Otto, F., Pinto, I., Pirani, A., Raghavan, K., Ranasinghe, R., Ruane, A., Ruiz, L., Sallée, J.-B., Samset, B., Sathyendranath, S., Seneviratne, S., Sörensson, A., Szopa, S., Takayabu, I., Tréguier, A.-M., van den Hurk, B., Vautard, R.,

https://doi.org/10.5194/egusphere-2026-2161
Preprint. Discussion started: 23 April 2026

von Schuckmann, K., Zaehle, S., Zhang, X., and Zickfeld, K.: Technical Summary, p. 33-144, Cambridge University Press, Cambridge, United Kingdom and New York, NY, USA, https://doi.org/10.1017/9781009157896.002, 2021.

Baars, H., Ansmann, A., Ohneiser, K., Haarig, M., Engelmann, R., Althausen, D., Hanssen, I., Gausa, M., Pietruczuk, A., Szkop, A., Stachlewska, I. S., Wang, D., Reichardt, J., Skupin, A., Mattis, I., Trickl, T., Vogelmann, H., Navas-Guzmán, F., Haefele, A., Acheson, K., Ruth, A. A., Tatarov, B., Müller, D., Hu, Q., Podvin, T., Goloub, P., Veselovskii, I., Pietras, C., Haeffelin, M., Fréville, P., Sicard, M., Comerón, A., Fernández García, A. J., Molero Menéndez, F., Córdoba-Jabonero, C., Guerrero-Rascado, J. L., Alados-Arboledas, L., Bortoli, D., Costa, M. J., Dionisi, D., Liberti, G. L., Wang, X., Sannino, A., Papagiannopoulos, N., Boselli, A., Mona, L., D'Amico, G., Romano, S., Perrone, M. R., Belegante, L., Nicolae, D., Grigorov, I., Gialitaki, A., Amiridis, V., Soupiona, O., Papayannis, A., Mamouri, R.-E., Nisantzi, A., Heese, B., Hofer, J., Schechner, Y. Y., Wandinger, U., and Pappalardo, G.: The unprecedented 2017–2018 stratospheric smoke event: decay phase and aerosol properties observed with the EARLINET, Atmospheric Chemistry and Physics, 19, 15 183–15 198, https://doi.org/10.5194/acp-19-15183-2019, 2019.

Barahona, D., Rodriguez, J., and Nenes, A.: Sensitivity of the global distribution of cirrus ice crystal concentration to heterogeneous freezing, Journal of Geophysical Research: Atmospheres, 115, https://doi.org/10.1029/2010JD014273, 2010.

Baumgardner, D., Dye, J. E., Gandrud, B. W., and Knollenberg, R. G.: Interpretation of measurements made by the forward scattering spectrometer probe (FSSP-300) during the Airborne Arctic Stratospheric Expedition, Journal of Geophysical Research: Atmospheres, 97, 8035–8046, https://doi.org/10.1029/91JD02728, 1992.

Baumgardner, D., Jonsson, H., Dawson, W., O'Connor, D., and Newton, R.: The cloud, aerosol and precipitation spectrometer: a new instrument for cloud investigations, Atmospheric Research, 59-60, 251–264, https://doi.org/10.1016/S0169-8095(01)00119-3, 2001.

Bock, L. and Burkhardt, U.: Contrail cirrus radiative forcing for future air traffic, Atmospheric Chemistry and Physics, 19, 8163–8174, https://doi.org/10.5194/acp-19-8163-2019, 2019.

Boucher, O., Randall, D., Artaxo, P., Bretherton, C., Feingold, G., Forster, P., Kerminen, V.-M., Kondo, Y., Liao, H., Lohmann, U., Rasch, P., Satheesh, S., Sherwood, S., Stevens, B., and Zhang, X.: Chapter 7: Clouds and Aerosols, pp. 571–658, Cambridge University Press, https://doi.org/10.1017/CBO9781107415324.016, 2013.

Bourassa, A. E., Rieger, L. A., Zawada, D. J., Khaykin, S., Thomason, L. W., and Degenstein, D. A.: Satellite Limb Observations of Unprecedented Forest Fire Aerosol in the Stratosphere, Journal of Geophysical Research: Atmospheres, 124, 9510–9519, https://doi.org/10.1029/2019jd030607, 2019.

Bräuer, T.: Flugzeuggetragene Messungen der Eigenschaften von Kondensstreifen aus Biotreibstoffgemischen, phdthesis, Universität der Bundeswehr München, https://doi.org/10.57676/pqt5-y634, 2021.

Bräuer, T., Voigt, C., Sauer, D., Kaufmann, S., Hahn, V., Scheibe, M., Schlager, H., Diskin, G. S., Nowak, J. B., DiGangi, J. P., Huber, F., Moore, R. H., and Anderson, B. E.: Airborne Measurements of Contrail Ice Properties—Dependence on Temperature and Humidity, Geophysical Research Letters, 48, https://doi.org/https://doi.org/10.1029/2020GL092166, 2021a.

Bräuer, T., Voigt, C., Sauer, D., Kaufmann, S., Hahn, V., Scheibe, M., Schlager, H., Huber, F., Le Clercq, P., Moore, R. H., and Anderson, B. E.: Reduced ice number concentrations in contrails from low-aromatic biofuel blends, Atmospheric Chemistry and Physics, 21, 16 817–16 826, https://doi.org/10.5194/acp-21-16817-2021, 2021b.

Brenguier, J.-L., Bourrianne, T., Coelho, A. A., Isbert, J., Peytavi, R., Trevarin, D., and Weschler, P.: Improvements of Droplet Size Distribution Measurements with the Fast-FSSP (Forward Scattering Spectrometer Probe), Journal of Atmospheric and Oceanic Technology, 15, 1077 – 1090, https://doi.org/10.1175/1520-0426(1998)015<1077:IODSDM>2.0.CO;2, 1998.

https://doi.org/10.5194/egusphere-2026-2161
Preprint. Discussion started: 23 April 2026

Brock, C. A., Hamill, P., Wilson, J. C., Jonsson, H. H., and Chan, K. R.: Particle Formation in the Upper Tropical Troposphere: A Source of Nuclei for the Stratospheric Aerosol, Science, 270, 1650–1653, https://doi.org/10.1126/science.270.5242.1650, 1995.

Brock, C. A., Froyd, K. D., Dollner, M., Williamson, C. J., Schill, G., Murphy, D. M., Wagner, N. J., Kupc, A., Jimenez, J. L., Campuzano-Jost, P., Nault, B. A., Schroder, J. C., Day, D. A., Price, D. J., Weinzierl, B., Schwarz, J. P., Katich, J. M., Wang, S., Zeng, L., Weber, R., Dibb, J., Scheuer, E., Diskin, G. S., DiGangi, J. P., Bui, T., Dean-Day, J. M., Thompson, C. R., Peischl, J., Ryerson, T. B., Bourgeois, I., Daube, B. C., Commane, R., and Wofsy, S. C.: Ambient aerosol properties in the remote atmosphere from global-scale in situ measurements, Atmospheric Chemistry and Physics, 21, 15 023–15 063, https://doi.org/10.5194/acp-21-15023-2021, 2021.

Burkhardt, U. and Kärcher, B.: Global radiative forcing from contrail cirrus, Nature Climate Change, 1, 54 – 58, https://doi.org/10.1038/nclimate1068, 2011.

Canagaratna, M., Jayne, J., Jimenez, J., Allan, J., Alfarra, M., Zhang, Q., Onasch, T., Drewnick, F., Coe, H., Middlebrook, A., Delia, A., Williams, L., Trimborn, A., Northway, M., DeCarlo, P., Kolb, C., Davidovits, P., and Worsnop, D.: Chemical and microphysical characterization of ambient aerosols with the aerodyne aerosol mass spectrometer, Mass Spectrometry Reviews, 26, 185–222, https://doi.org/https://doi.org/10.1002/mas.20115, 2007.

Clemen, H.-C. et al.: Indications for non-soot aircraft emissions in cloud residuals and aerosol particles, in prep. for Atmospheric Chemistry and Physics, in prep.

Cziczo, D. J. and Froyd, K. D.: Sampling the composition of cirrus ice residuals, Atmospheric Research, 142, 15–31, https://doi.org/10.1016/j.atmosres.2013.06.012, 2014.

Cziczo, D. J., Murphy, D. M., Hudson, P. K., and Thomson, D. S.: Single particle measurements of the chemical composition of cirrus ice residue during CRYSTAL-FACE, Journal of Geophysical Research: Atmospheres, 109, https://doi.org/10.1029/2003JD004032, 2004.

Cziczo, D. J., Froyd, K. D., Hoose, C., Jensen, E. J., Diao, M., Zondlo, M. A., Smith, J. B., Twohy, C. H., and Murphy, D. M.: Clarifying the Dominant Sources and Mechanisms of Cirrus Cloud Formation, Science, 340, 1320–1324, https://doi.org/10.1126/science.1234145, 2013.

Damoah, R., Spichtinger, N., Servranckx, R., Fromm, M., Eloranta, E. W., Razenkov, I. A., James, P., Shulski, M., Forster, C., and Stohl, A.: A case study of pyro-convection using transport model and remote sensing data, Atmospheric Chemistry and Physics, 6, 173–185, https://doi.org/10.5194/acp-6-173-2006, 2006.

Dischl, R., Sauer, D., Voigt, C., Harlaß, T., Sakellariou, F., Märkl, R., Schumann, U., Scheibe, M., Kaufmann, S., Roiger, A., Dörnbrack, A., Renard, C., Gauthier, M., Swann, P., Madden, P., Luff, D., Johnson, M., Ahrens, D., Sallinen, R., Schripp, T., Eckel, G., Bauder, U., and Le Clercq, P.: Measurements of particle emissions of an A350-941 burning 100 aviation fuels in cruise, Atmospheric Chemistry and Physics, 24, 11 255–11 273, https://doi.org/10.5194/acp-24-11255-2024, 2024.

Dischl, R., Märkl, R., Sauer, D., Voigt, C., Harlaß, T., Scheibe, M., Hahn, V., Kaufmann, S., Marsing, A., Dörnbrack, A., Roiger, A., Yu, F., Gauthier, M., Renard, C., Swann, P., Johnson, M., Ahrens, D., Sallinen, R., Eckel, G., and Clercq, P. L.: Fuel sulfur content can modulate contrail ice crystal numbers, https://doi.org/10.21203/rs.3.rs-6566706/v1, 2025.

Ditas, J., Ma, N., Zhang, Y., Assmann, D., Neumaier, M., Riede, H., Karu, E., Williams, J., Scharffe, D., Wang, Q., Saturno, J., Schwarz, J. P., Katich, J. M., McMeeking, G. R., Zahn, A., Hermann, M., Brenninkmeijer, C. A. M., Andreae, M. O., Pöschl, U., Su, H., and Cheng, Y.: Strong impact of wildfires on the abundance and aging of black carbon in the lowermost stratosphere, Proceedings of the National Academy of Sciences, 115, E11 595–E11 603, https://doi.org/10.1073/pnas.1806868115, 2018.

DMT: CAPS CLOUD, AEROSOL AND PRECIPITATION SPECTROMETER, https://www.envicontrol.com/storage/app/media/uploaded-files/CAPSBrochure.pdf, 2014.

https://doi.org/10.5194/egusphere-2026-2161
Preprint. Discussion started: 23 April 2026

Dragoneas, A., Molleker, S., Appel, O., Hünig, A., Böttger, T., Hermann, M., Drewnick, F., Schneider, J., Weigel, R., and Borrmann, S.: The realization of autonomous, aircraft-based, real-time aerosol mass spectrometry in the upper troposphere and lower stratosphere, Atmospheric Measurement Techniques, 15, 5719–5742, https://doi.org/10.5194/amt-15-5719-2022, 2022.

Drewnick, F., Hings, S. S., DeCarlo, P., Jayne, J. T., Gonin, M., Fuhrer, K., Weimer, S., Jimenez, J. L., Demerjian, K. L., Borrmann, S., and Worsnop, D. R.: A New Time-of-Flight Aerosol Mass Spectrometer (TOF-AMS)—Instrument Description and First Field Deployment, Aerosol Science and Technology, 39, 637–658, https://doi.org/10.1080/02786820500182040, 2005.

Eppers, O., Köllner, F., Appel, O., Brauner, P., Ekinci, F., Molleker, S., Dragoneas, A., Smith, W., Ueyama, R., Bucci, S., Legras, B., Williamson, C., Pan, L., Cheng, Y., and S. Borrmann, S.: Regional contributions to the chemical composition of the Asian tropopause aerosol layer (ATAL), under review in Journal of Geophysical Research: Atmospheres, 2025.

Franklin, J. E., Drummond, J. R., Griffin, D., Pierce, J. R., Waugh, D. L., Palmer, P. I., Parrington, M., Lee, J. D., Lewis, A. C., Rickard, A. R., Taylor, J. W., Allan, J. D., Coe, H., Walker, K. A., Chisholm, L., Duck, T. J., Hopper, J. T., Blanchard, Y., Gibson, M. D., Curry, K. R., Sakamoto, K. M., Lesins, G., Dan, L., Kliever, J., and Saha, A.: A case study of aerosol scavenging in a biomass burning plume over eastern Canada during the 2011 BORTAS field experiment, Atmospheric Chemistry and Physics, 14, 8449–8460, https://doi.org/10.5194/acp-14-8449-2014, 2014.

Fromm, M. D. and Servranckx, R.: Transport of forest fire smoke above the tropopause by supercell convection, Geophysical Research Letters, 30, https://doi.org/10.1029/2002GL016820, 2003.

Froyd, K., Yu, P., Schill, G., Brock, C., Kupc, A., Williamson, C., Jensen, E., Ray, E., Rosenlof, K., Bian, H., Darmenov, A., Colarco, P., Diskin, G., Bui, T., and Murphy, D.: Dominant Role of Mineral Dust in Cirrus Cloud Formation, Nature Geoscience, 15, 177–183, https://doi.org/10.1038/s41561-022-00901-w, 2022.

Gayet, J.-F., Shcherbakov, V., Voigt, C., Schumann, U., Schäuble, D., Jessberger, P., Petzold, A., Minikin, A., Schlager, H., Dubovik, O., and Lapyonok, T.: The evolution of microphysical and optical properties of an A380 contrail in the vortex phase, Atmospheric Chemistry and Physics, 12, 6629–6643, https://doi.org/10.5194/acp-12-6629-2012, 2012.

Gettelman, A., Hoor, P., Pan, L. L., Randel, W. J., Hegglin, M. I., and Birner, T.: THE EXTRATROPICAL UPPER TROPOSPHERE AND LOWER STRATOSPHERE, Reviews of Geophysics, 49, https://doi.org/10.1029/2011rg000355, 2011.

Hersbach, H., Bell, B., Berrisford, P., Biavati, G., Horányi, A., Muñoz Sabater, J., Nicolas, J., Peubey, C., Radu, R., Rozum, I., Schepers, D., Simmons, A., Soci, C., Dee, D., and Thépaut, J.-N.: ERA5 hourly data on pressure levels from 1940 to present, https://doi.org/10.24381/cds.bd0915c6, 2018.

Hersbach, H., Bell, B., Berrisford, P., Hirahara, S., Horányi, A., Muñoz-Sabater, J., Nicolas, J., Peubey, C., Radu, R., Schepers, D., Simmons, A., Soci, C., Abdalla, S., Abellan, X., Balsamo, G., Bechtold, P., Biavati, G., Bidlot, J., Bonavita, M., De Chiara, G., Dahlgren, P., Dee, D., Diamantakis, M., Dragani, R., Flemming, J., Forbes, R., Fuentes, M., Geer, A., Haimberger, L., Healy, S., Hogan, R. J., Hólm, E., Janisková, M., Keeley, S., Laloyaux, P., Lopez, P., Lupu, C., Radnoti, G., de Rosnay, P., Rozum, I., Vamborg, F., Villaume, S., and Thépaut, J.: The ERA5 global reanalysis, Quarterly Journal of the Royal Meteorological Society, 146, 1999–2049, https://doi.org/10.1002/qj.3803, 2020.

Heymsfield, A., Baumgardner, D., DeMott, P., Forster, P., Gierens, K., and Kärcher, B.: Contrail Microphysics, Bulletin of the American Meteorological Society, 91, 465 – 472, https://doi.org/10.1175/2009BAMS2839.1, 2010.

Heymsfield, A. J., Krämer, M., Luebke, A., Brown, P., Cziczo, D. J., Franklin, C., Lawson, P., Lohmann, U., McFarquhar, G., Ulanowski, Z., and Tricht, K. V.: Cirrus Clouds, Meteorological Monographs, 58, 2.1 – 2.26, https://doi.org/10.1175/AMSMONOGRAPHS-D-16-0010.1, 2017.

https://doi.org/10.5194/egusphere-2026-2161
Preprint. Discussion started: 23 April 2026

Hinz, K.-P., Kaufmann, R., and Spengler, B.: Laser-Induced Mass Analysis of Single Particles in the Airborne State, Analytical Chemistry, 66, 2071–2076, https://doi.org/10.1021/ac00085a023, 1994.

Hinz, K. P., Greweling, M., Drews, F., and Spengler, B.: Data processing in on-line laser mass spectrometry of inorganic, organic, or biological airborne particles, Journal of the American Society for Mass Spectrometry, 10, 648–660, https://doi.org/10.1016/S1044-0305(99)00028-8, 1999.

Homeyer, C. R., McAuliffe, J. D., and Bedka, K. M.: On the Development of Above-Anvil Cirrus Plumes in Extratropical Convection, Journal of the Atmospheric Sciences, 74, 1617–1633, https://doi.org/10.1175/jas-d-16-0269.1, 2017.

Hoose, C., Lohmann, U., Erdin, R., and Tegen, I.: The global influence of dust mineralogical composition on heterogeneous ice nucleation in mixed-phase clouds, Environmental Research Letters, 3, 025 003, https://doi.org/10.1088/1748-9326/3/2/025003, 2008.

Hünig, A.: Development, characterization, and first field deploymentsof a novel aerosol mass spectrometer combining laserablation and flash vaporization techniques for aircraftapplication at high altitudes, phdthesis, Johannes Gutenberg Universität, https://doi.org/10.25358/openscience-5554, 2020.

Hünig, A., Appel, O., Dragoneas, A., Molleker, S., Clemen, H.-C., Helleis, F., Klimach, T., Köllner, F., Böttger, T., Drewnick, F., Schneider, J., and Borrmann, S.: Design, characterization, and first field deployment of a novel aircraft-based aerosol mass spectrometer combining the laser ablation and flash vaporization techniques, Atmospheric Measurement Techniques, 15, 2889–2921, https://doi.org/10.5194/amt-15-2889-2022, 2022.

Höpfner, M., Volkamer, R., Grabowski, U., Grutter, M., Orphal, J., Stiller, G., von Clarmann, T., and Wetzel, G.: First detection of ammonia (NH3) in the Asian summer monsoon upper troposphere, Atmospheric Chemistry and Physics, 16, 14 357–14 369, https://doi.org/10.5194/acp-16-14357-2016, 2016.

Höpfner, M., Ungermann, J., Borrmann, S., Wagner, R., Spang, R., Riese, M., Stiller, G., Appel, O., Batenburg, A. M., Bucci, S., Cairo, F., Dragoneas, A., Friedl-Vallon, F., Hünig, A., Johansson, S., Krasauskas, L., Legras, B., Leisner, T., Mahnke, C., Möhler, O., Molleker, S., Müller, R., Neubert, T., Orphal, J., Preusse, P., Rex, M., Saathoff, H., Stroh, F., Weigel, R., and Wohltmann, I.: Ammonium nitrate particles formed in upper troposphere from ground ammonia sources during Asian monsoons, Nature Geoscience, 12, 608–612, https://doi.org/10.1038/s41561-019-0385-8, 2019.

Jackson, R. C., McFarquhar, G. M., Fridlind, A. M., and Atlas, R.: The dependence of cirrus gamma size distributions expressed as volumes in N_0-λ-μ phase space and bulk cloud properties on environmental conditions: Results from the Small Ice Particles in Cirrus Experiment (SPARTICUS), Journal of Geophysical Research: Atmospheres, 120, 10,351–10,377, https://doi.org/10.1002/2015JD023492, 2015.

Jahl, L. G., Brubaker, T. A., Polen, M. J., Jahn, L. G., Cain, K. P., Bowers, B. B., Fahy, W. D., Graves, S., and Sullivan, R. C.: Atmospheric aging enhances the ice nucleation ability of biomass-burning aerosol, Science Advances, 7, https://doi.org/10.1126/sciadv.abd3440, 2021.

Jensen, E. J., Smith, J. B., Pfister, L., Pittman, J. V., Weinstock, E. M., Sayres, D. S., Herman, R. L., Troy, R. F., Rosenlof, K., Thompson, T. L., Fridlind, A. M., Hudson, P. K., Cziczo, D. J., Heymsfield, A. J., Schmitt, C., and Wilson, J. C.: Ice supersaturations exceeding 100tropical tropopause: implications for cirrus formation and dehydration, Atmospheric Chemistry and Physics, 5, 851–862, https://doi.org/10.5194/acp-5-851-2005, 2005.

Jolleys, M. D., Coe, H., McFiggans, G., Taylor, J. W., O'Shea, S. J., Le Breton, M., Bauguitte, S. J.-B., Moller, S., Di Carlo, P., Aruffo, E., Palmer, P. I., Lee, J. D., Percival, C. J., and Gallagher, M. W.: Properties and evolution of biomass burning organic aerosol from Canadian boreal forest fires, Atmospheric Chemistry and Physics, 15, 3077–3095, https://doi.org/10.5194/acp-15-3077-2015, 2015.

Joppe, P., Schneider, J., Wilsch, J., Bozem, H., Breuninger, A., Curtius, J., Ebert, M., Emig, N., Hoor, P., Ismayil, S., Kandler, K., Kunkel, D., Kurth, I., Lachnitt, H.-C., Li, Y., Miltenberger, A., Richter, S., Rolf, C., Schneider, L., Schwenk, C., Spelten, N., Vogel, A. L., Cheng,

https://doi.org/10.5194/egusphere-2026-2161
Preprint. Discussion started: 23 April 2026

Y., and Borrmann, S.: Transport of Biomass Burning Aerosol into the Extratropical Tropopause Region over Europe via Warm Conveyor Belt Uplift, EGUsphere, 2025, 1–39, https://doi.org/10.5194/egusphere-2025-1346, 2025.

Junge, C. E., Chagnon, C. W., and Manson, J. E.: STRATOSPHERIC AEROSOLS, Journal of Atmospheric Sciences, 18, 81 – 108, https://doi.org/10.1175/1520-0469(1961)018<0081:SA>2.0.CO;2, 1961.

Kaluza, T., Kunkel, D., and Hoor, P.: On the occurrence of strong vertical wind shear in the tropopause region: a 10-year ERA5 northern hemispheric study, Weather and Climate Dynamics, 2, 631–651, https://doi.org/10.5194/wcd-2-631-2021, 2021.

Kanji, Z. A., Ladino, L. A., Wex, H., Boose, Y., Burkert-Kohn, M., Cziczo, D. J., and Krämer, M.: Overview of Ice Nucleating Particles, Meteorological Monographs, 58, 1.1 – 1.33, https://doi.org/10.1175/AMSMONOGRAPHS-D-16-0006.1, 2017.

Kärcher, B.: Formation and radiative forcing of contrail cirrus, Nature Communications, 9, 1824, https://doi.org/10.1038/s41467-018-04068-0, 2018.

Karydis, V. A., Kumar, P., Barahona, D., Sokolik, I. N., and Nenes, A.: On the effect of dust particles on global cloud condensation nuclei and cloud droplet number, Journal of Geophysical Research: Atmospheres, 116, https://doi.org/10.1029/2011JD016283, 2011.

Kaufmann, S., Voigt, C., Jurkat, T., Thornberry, T., Fahey, D. W., Gao, R.-S., Schlage, R., Schäuble, D., and Zöger, M.: The airborne mass spectrometer AIMS – Part 1: AIMS-H2O for UTLS water vapor measurements, Atmospheric Measurement Techniques, 9, 939–953, https://doi.org/10.5194/amt-9-939-2016, 2016.

Kelly, J. T., Chuang, C. C., and Wexler, A. S.: Influence of dust composition on cloud droplet formation, Atmospheric Environment, 41, 2904–2916, https://doi.org/10.1016/j.atmosenv.2006.12.008, 2007.

Kelso, N. and Patterson, T.: Free vector and raster map data, https://www.naturalearthdata.com/, 2025.

Khaykin, S. M., Godin-Beekmann, S., Hauchecorne, A., Pelon, J., Ravetta, F., and Keckhut, P.: Stratospheric Smoke With Unprecedentedly High Backscatter Observed by Lidars Above Southern France, Geophysical Research Letters, 45, 1639–1646, https://doi.org/10.1002/2017gl076763, 2018.

Klimach, T.: Chemische Zusammensetzung der Aerosole : Design und Datenauswertung eines Einzelpartikel-Laserablationsmassenspektrometers, Ph.D. thesis, Mainz, https://doi.org/10.25358/openscience-4386, 2012.

Klingebiel, M., de Lozar, A., Molleker, S., Weigel, R., Roth, A., Schmidt, L., Meyer, J., Ehrlich, A., Neuber, R., Wendisch, M., and Borrmann, S.: Arctic low-level boundary layer clouds: in situ measurements and simulations of mono- and bimodal supercooled droplet size distributions at the top layer of liquid phase clouds, Atmospheric Chemistry and Physics, 15, 617–631, https://doi.org/10.5194/acp-15-617-2015, 2015.

Kloss, C., Berthet, G., Sellitto, P., Ploeger, F., Bucci, S., Khaykin, S., Jégou, F., Taha, G., Thomason, L. W., Barret, B., Le Flochmoen, E., von Hobe, M., Bossolasco, A., Bègue, N., and Legras, B.: Transport of the 2017 Canadian wildfire plume to the tropics via the Asian monsoon circulation, Atmospheric Chemistry and Physics, 19, 13 547–13 567, https://doi.org/10.5194/acp-19-13547-2019, 2019.

Krämer, M., Schiller, C., Afchine, A., Bauer, R., Gensch, I., Mangold, A., Schlicht, S., Spelten, N., Sitnikov, N., Borrmann, S., de Reus, M., and Spichtinger, P.: Ice supersaturations and cirrus cloud crystal numbers, Atmospheric Chemistry and Physics, 9, 3505–3522, https://doi.org/10.5194/acp-9-3505-2009, 2009.

Krämer, M., Rolf, C., Luebke, A., Afchine, A., Spelten, N., Costa, A., Meyer, J., Zöger, M., Smith, J., Herman, R. L., Buchholz, B., Ebert, V., Baumgardner, D., Borrmann, S., Klingebiel, M., and Avallone, L.: A microphysics guide to cirrus clouds – Part 1: Cirrus types, Atmospheric Chemistry and Physics, 16, 3463–3483, https://doi.org/10.5194/acp-16-3463-2016, 2016.

Krämer, M., Rolf, C., Spelten, N., Afchine, A., Fahey, D., Jensen, E., Khaykin, S., Kuhn, T., Lawson, P., Lykov, A., Pan, L. L., Riese, M., Rollins, A., Stroh, F., Thornberry, T., Wolf, V., Woods, S., Spichtinger, P., Quaas, J., and Sourdeval, O.: A microphysics guide

https://doi.org/10.5194/egusphere-2026-2161
Preprint. Discussion started: 23 April 2026

to cirrus – Part 2: Climatologies of clouds and humidity from observations, Atmospheric Chemistry and Physics, 20, 12 569–12 608, https://doi.org/10.5194/acp-20-12569-2020, 2020.

Kremser, S., Thomason, L. W., von Hobe, M., Hermann, M., Deshler, T., Timmreck, C., Toohey, M., Stenke, A., Schwarz, J. P., Weigel, R., Fueglistaler, S., Prata, F. J., Vernier, J.-P., Schlager, H., Barnes, J. E., Antuña-Marrero, J.-C., Fairlie, D., Palm, M., Mahieu, E., Notholt, J., Rex, M., Bingen, C., Vanhellemont, F., Bourassa, A., Plane, J. M. C., Klocke, D., Carn, S. A., Clarisse, L., Trickl, T., Neely, R., James, A. D., Rieger, L., Wilson, J. C., and Meland, B.: Stratospheric aerosol—Observations, processes, and impact on climate, Reviews of Geophysics, 54, 278–335, https://doi.org/10.1002/2015RG000511, 2016.

Kunkel, D., Hoor, P., Kaluza, T., Ungermann, J., Kluschat, B., Giez, A., Lachnitt, H.-C., Kaufmann, M., and Riese, M.: Evidence of small-scale quasi-isentropic mixing in ridges of extratropical baroclinic waves, Atmospheric Chemistry and Physics, 19, 12 607–12 630, https://doi.org/10.5194/acp-19-12607-2019, 2019.

Labitzke, K. and McCormick, M. P.: Stratospheric temperature increases due to Pinatubo aerosols, Geophysical Research Letters, 19, 207–210, https://doi.org/10.1029/91GL02940, 1992.

Lachnitt, H.-C., Hoor, P., Kunkel, D., Bramberger, M., Dörnbrack, A., Müller, S., Reutter, P., Giez, A., Kaluza, T., and Rapp, M.: Gravity-wave-induced cross-isentropic mixing: a DEEPWAVE case study, Atmospheric Chemistry and Physics, 23, 355–373, https://doi.org/10.5194/acp-23-355-2023, 2023.

Lawson, R. P., Baker, B., Pilson, B., and Mo, Q.: In Situ Observations of the Microphysical Properties of Wave, Cirrus, and Anvil Clouds. Part II: Cirrus Clouds, Journal of the Atmospheric Sciences, 63, 3186 – 3203, https://doi.org/10.1175/JAS3803.1, 2006.

Lee, J.-Y., Marotzke, J., Bala, G., Cao, L., Corti, S., Dunne, J., Engelbrecht, F., Fischer, E., Fyfe, J., Jones, C., Maycock, A., Mutemi, J., Ndiaye, O., Panickal, S., and Zhou, T.: Future Global Climate: Scenario-Based Projections and Near-Term Information, p. 553–672, Cambridge University Press, Cambridge, United Kingdom and New York, NY, USA, https://doi.org/10.1017/9781009157896.006, 2021.

Levin, Z., Teller, A., Ganor, E., and Yin, Y.: On the interactions of mineral dust, sea-salt particles, and clouds: A measurement and modeling study from the Mediterranean Israeli Dust Experiment campaign, Journal of Geophysical Research: Atmospheres, 110, https://doi.org/10.1029/2005JD005810, 2005.

Liou, K.-N.: Influence of Cirrus Clouds on Weather and Climate Processes: A Global Perspective, Monthly Weather Review, 114, 1167 – 1199, https://doi.org/10.1175/1520-0493(1986)114<1167:IOCCOW>2.0.CO;2, 1986.

Luebke, A. E., Afchine, A., Costa, A., Grooß, J.-U., Meyer, J., Rolf, C., Spelten, N., Avallone, L. M., Baumgardner, D., and Krämer, M.: The origin of midlatitude ice clouds and the resulting influence on their microphysical properties, Atmospheric Chemistry and Physics, 16, 5793–5809, https://doi.org/10.5194/acp-16-5793-2016, 2016.

Mahrt, F., Marcolli, C., David, R. O., Grönquist, P., Barthazy Meier, E. J., Lohmann, U., and Kanji, Z. A.: Ice nucleation abilities of soot particles determined with the Horizontal Ice Nucleation Chamber, Atmospheric Chemistry and Physics, 18, 13 363–13 392, https://doi.org/10.5194/acp-18-13363-2018, 2018.

Mahrt, F., Kilchhofer, K., Marcolli, C., Grönquist, P., David, R. O., Rösch, M., Lohmann, U., and Kanji, Z. A.: The Impact of Cloud Processing on the Ice Nucleation Abilities of Soot Particles at Cirrus Temperatures, Journal of Geophysical Research: Atmospheres, 125, https://doi.org/10.1029/2019JD030922, 2020.

Martinsson, B. G., Friberg, J., Sandvik, O. S., Hermann, M., van Velthoven, P. F. J., and Zahn, A.: Formation and composition of the UTLS aerosol, npj Climate and Atmospheric Science, 2, https://doi.org/10.1038/s41612-019-0097-1, 2019.

McCormick, M., Thomason, L., and Trepte, C.: Atmospheric effects of the Mt Pinatubo eruption, Nature, 373, 399–404, https://doi.org/10.1038/373399a0, 1995.

https://doi.org/10.5194/egusphere-2026-2161
Preprint. Discussion started: 23 April 2026

Moore, K. G., Clarke, A. D., Kapustin, V. N., McNaughton, C., Anderson, B. E., Winstead, E. L., Weber, R., Ma, Y., Lee, Y. N., Talbot, R., Dibb, J., Anderson, T., Doherty, S., Covert, D., and Rogers, D.: A comparison of similar aerosol measurements made on the NASA P3-B, DC-8, and NSF C-130 aircraft during TRACE-P and ACE-Asia, Journal of Geophysical Research (Atmospheres), 109, D15S15, https://doi.org/10.1029/2003JD003543, 2004.

Moore, R. H., Thornhill, K. L., Weinzierl, B., Sauer, D., D'Ascoli, E., Kim, J., Lichtenstern, M., Scheibe, M., Beaton, B., Beyersdorf, A. j., Bulzan, D., Corr, C. A., Crosbie, E., Jurkat, T., Martin, R., Riddick, D., Shook, M., Slover, G., Voigt, C., White, R., Winstead, E., Yasky, R., Ziemba, L. D., Brown, A., Schlager, H., and Anderson, B. E.: Biofuel blending reduces particle emissions from aircraft engines at cruise conditions, Nature, 543, 411–415, https://doi.org/10.1038/nature21420, 2017.

Moore, R. H., Wiggins, E. B., Ahern, A. T., Zimmerman, S., Montgomery, L., Campuzano Jost, P., Robinson, C. E., Ziemba, L. D., Winstead, E. L., Anderson, B. E., Brock, C. A., Brown, M. D., Chen, G., Crosbie, E. C., Guo, H., Jimenez, J. L., Jordan, C. E., Lyu, M., Nault, B. A., Rothfuss, N. E., Sanchez, K. J., Schueneman, M., Shingler, T. J., Shook, M. A., Thornhill, K. L., Wagner, N. L., and Wang, J.: Sizing response of the Ultra-High Sensitivity Aerosol Spectrometer (UHSAS) and Laser Aerosol Spectrometer (LAS) to changes in submicron aerosol composition and refractive index, Atmospheric Measurement Techniques, 14, 4517–4542, https://doi.org/10.5194/amt-14-4517-2021, 2021.

Muhlbauer, A., Ackerman, T. P., Comstock, J. M., Diskin, G. S., Evans, S. M., Lawson, R. P., and Marchand, R. T.: Impact of large-scale dynamics on the microphysical properties of midlatitude cirrus, Journal of Geophysical Research: Atmospheres, 119, 3976–3996, https://doi.org/10.1002/2013JD020035, 2014.

Murphy, D. M. and Thomson, D. S.: Laser Ionization Mass Spectroscopy of Single Aerosol Particles, Aerosol Science and Technology, 22, 237–249, https://doi.org/10.1080/02786829408959743, 1995.

Murphy, D. M., Thomson, D. S., and Mahoney, M. J.: In Situ Measurements of Organics, Meteoritic Material, Mercury, and Other Elements in Aerosols at 5 to 19 Kilometers, Science, 282, 1664–1669, https://doi.org/10.1126/science.282.5394.1664, 1998.

Myhre, G., Myhre, C. E., Samset, B. H., and Storelvmo, T.: Aerosols and their Relation to Global Climate and Climate Sensitivity, https://www.nature.com/scitable/knowledge/library/aerosols-and-their-relation-to-global-climate-102215345/, 2013.

Märkl, R. S., Voigt, C., Sauer, D., Dischl, R. K., Kaufmann, S., Harlaß, T., Hahn, V., Roiger, A., Weiß-Rehm, C., Burkhardt, U., Schumann, U., Marsing, A., Scheibe, M., Dörnbrack, A., Renard, C., Gauthier, M., Swann, P., Madden, P., Luff, D., Sallinen, R., Schripp, T., and Le Clercq, P.: Powering aircraft with 100 Atmospheric Chemistry and Physics, 24, 3813–3837, https://doi.org/10.5194/acp-24-3813-2024, 2024.

Ng, N. L., Canagaratna, M. R., Zhang, Q., Jimenez, J. L., Tian, J., Ulbrich, I. M., Kroll, J. H., Docherty, K. S., Chhabra, P. S., Bahreini, R., Murphy, S. M., Seinfeld, J. H., Hildebrandt, L., Donahue, N. M., DeCarlo, P. F., Lanz, V. A., Prévôt, A. S. H., Dinar, E., Rudich, Y., and Worsnop, D. R.: Organic aerosol components observed in Northern Hemispheric datasets from Aerosol Mass Spectrometry, Atmospheric Chemistry and Physics, 10, 4625–4641, https://doi.org/10.5194/acp-10-4625-2010, 2010.

Ng, N. L., Canagaratna, M. R., Jimenez, J. L., Chhabra, P. S., Seinfeld, J. H., and Worsnop, D. R.: Changes in organic aerosol composition with aging inferred from aerosol mass spectra, Atmospheric Chemistry and Physics, 11, 6465–6474, https://doi.org/10.5194/acp-11-6465-2011, 2011.

NOAA-NCEI: Monthly Wildfires Report for January 2018, https://www.ncei.noaa.gov/access/monitoring/monthly-report/fire/201801, 2018.

O'Dowd, C., Smith, M., Consterdine, I., and Lowe, J.: Marine aerosol, sea-salt, and the marine sulphur cycle: a short review, Atmospheric Environment, 31, 73–80, https://doi.org/10.1016/S1352-2310(96)00106-9, 1997.

https://doi.org/10.5194/egusphere-2026-2161
Preprint. Discussion started: 23 April 2026

Onasch, T. B., Jayne, J. T., Herndon, S., Worsnop, D. R., Miake-Lye, R. C., Mortimer, I. P., and Anderson, B. E.: Chemical Properties of Aircraft Engine Particulate Exhaust Emissions, Journal of Propulsion and Power, 25, 1121–1137, https://doi.org/10.2514/1.36371, 2009.

Patnaude, R. J., Moore, K. A., Perkins, R. J., Hill, T. C. J., DeMott, P. J., and Kreidenweis, S. M.: Low-temperature ice nucleation of sea spray and secondary marine aerosols under cirrus cloud conditions, Atmospheric Chemistry and Physics, 24, 911–928, https://doi.org/10.5194/acp-24-911-2024, 2024.

Peterson, D. A., Campbell, J. R., Hyer, E. J., Fromm, M. D., Kablick, G. P., Cossuth, J. H., and DeLand, M. T.: Wildfire-driven thunderstorms cause a volcano-like stratospheric injection of smoke, npj Climate and Atmospheric Science, 1, https://doi.org/10.1038/s41612-018-0039-3, 2018.

Pierce, J. R. and Adams, P. J.: Global evaluation of CCN formation by direct emission of sea salt and growth of ultrafine sea salt, Journal of Geophysical Research: Atmospheres, 111, https://doi.org/10.1029/2005JD006186, 2006.

Ploeger, F., Konopka, P., Müller, R., Fueglistaler, S., Schmidt, T., Manners, J. C., Grooß, J., Günther, G., Forster, P. M., and Riese, M.: Horizontal transport affecting trace gas seasonality in the Tropical Tropopause Layer (TTL), Journal of Geophysical Research: Atmospheres, 117, https://doi.org/10.1029/2011jd017267, 2012.

Poberaj, C. S., Staehelin, J., and Brunner, D.: Missing Stratospheric Ozone Decrease at Southern Hemisphere Middle Latitudes after Mt. Pinatubo: A Dynamical Perspective, Journal of the Atmospheric Sciences, 68, 1922 – 1945, https://doi.org/10.1175/JAS-D-10-05004.1, 2011.

Prather, K. A., Nordmeyer, T., and Salt, K.: Real-time characterization of individual aerosol particles using time-of-flight mass spectrometry, Analytical Chemistry, 66, 1403–1407, https://doi.org/10.1021/ac00081a007, 1994.

Pratt, K. A. and Prather, K. A.: Aircraft measurements of vertical profiles of aerosol mixing states, Journal of Geophysical Research: Atmospheres, 115, https://doi.org/10.1029/2009JD013150, 2010.

Pratt, K. A., Mayer, J. E., Holecek, J. C., Moffet, R. C., Sanchez, R. O., Rebotier, T. P., Furutani, H., Gonin, M., Fuhrer, K., Su, Y., Guazzotti, S., and Prather, K. A.: Development and Characterization of an Aircraft Aerosol Time-of-Flight Mass Spectrometer, Analytical Chemistry, 81, 1792–1800, https://doi.org/10.1021/ac801942r, 2009.

Randel, W. and Jensen, E.: Physical processes in the tropical tropopause layer and their roles in a changing climate., Nature Geoscience, 6, 169–176, https://doi.org/10.1038/ngeo1733, 2013.

Randel, W. J. and Park, M.: Deep convective influence on the Asian summer monsoon anticyclone and associated tracer variability observed with Atmospheric Infrared Sounder (AIRS), Journal of Geophysical Research: Atmospheres, 111, https://doi.org/10.1029/2005jd006490, 2006.

Reutter, P., Škerlak, B., Sprenger, M., and Wernli, H.: Stratosphere–troposphere exchange (STE) in the vicinity of North Atlantic cyclones, Atmospheric Chemistry and Physics, 15, 10 939–10 953, https://doi.org/10.5194/acp-15-10939-2015, 2015.

Richardson, M. S., DeMott, P. J., Kreidenweis, S. M., Cziczo, D. J., Dunlea, E. J., Jimenez, J. L., Thomson, D. S., Ashbaugh, L. L., Borys, R. D., Westphal, D. L., Casuccio, G. S., and Lersch, T. L.: Measurements of heterogeneous ice nuclei in the western United States in springtime and their relation to aerosol characteristics, Journal of Geophysical Research: Atmospheres, 112, https://doi.org/10.1029/2006JD007500, 2007.

Riese, M., Ploeger, F., Rap, A., Vogel, B., Konopka, P., Dameris, M., and Forster, P.: Impact of uncertainties in atmospheric mixing on simulated UTLS composition and related radiative effects, Journal of Geophysical Research: Atmospheres, 117, https://doi.org/10.1029/2012jd017751, 2012.

https://doi.org/10.5194/egusphere-2026-2161
Preprint. Discussion started: 23 April 2026

Roth, A., Schneider, J., Klimach, T., Mertes, S., van Pinxteren, D., Herrmann, H., and Borrmann, S.: Aerosol properties, source identification, and cloud processing in orographic clouds measured by single particle mass spectrometry on a central European mountain site during HCCT-2010, Atmospheric Chemistry and Physics, 16, 505–524, https://doi.org/10.5194/acp-16-505-2016, 2016.

Sakamoto, K. M., Allan, J. D., Coe, H., Taylor, J. W., Duck, T. J., and Pierce, J. R.: Aged boreal biomass-burning aerosol size distributions from BORTAS 2011, Atmospheric Chemistry and Physics, 15, 1633–1646, https://doi.org/10.5194/acp-15-1633-2015, 2015.

Santer, B. D., Bonfils, C., Painter, J. F., Zelinka, M. D., Mears, C., Solomon, S., Schmidt, G. A., Fyfe, J. C., Cole, J. N. S., Nazarenko, L., Taylor, K. E., and Wentz, F. J.: Volcanic contribution to decadal changes in tropospheric temperature, Nature Geoscience, 7, 185–189, https://doi.org/10.1038/ngeo2098, 2014.

Savitzky, A. and Golay, M. J. E.: Smoothing and Differentiation of Data by Simplified Least Squares Procedures., Analytical Chemistry, 36, 1627–1639, https://doi.org/10.1021/ac60214a047, 1964.

Schill, G. P., Froyd, K. D., Bian, H., Kupc, A., Williamson, C., Brock, C. A., Ray, E., Hornbrook, R. S., Hills, A. J., Apel, E. C., Chin, M., Colarco, P. R., and Murphy, D. M.: Widespread biomass burning smoke throughout the remote troposphere, Nature Geoscience, 13, 422–427, https://doi.org/10.1038/s41561-020-0586-1, 2020.

Schiller, C., Krämer, M., Afchine, A., Spelten, N., and Sitnikov, N.: Ice water content of Arctic, midlatitude, and tropical cirrus, Journal of Geophysical Research: Atmospheres, 113, https://doi.org/10.1029/2008jd010342, 2008.

Schneider, J., Weigel, R., Klimach, T., Dragoneas, A., Appel, O., Hünig, A., Molleker, S., Köllner, F., Clemen, H.-C., Eppers, O., Hoppe, P., Hoor, P., Mahnke, C., Krämer, M., Rolf, C., Grooß, J.-U., Zahn, A., Obersteiner, F., Ravegnani, F., Ulanovsky, A., Schlager, H., Scheibe, M., Diskin, G. S., DiGangi, J. P., Nowak, J. B., Zöger, M., and Borrmann, S.: Aircraft-based observation of meteoric material in lower-stratospheric aerosol particles between 15 and 68° N, Atmospheric Chemistry and Physics, 21, 989–1013, https://doi.org/10.5194/acp-21-989-2021, 2021.

Schripp, T., Anderson, B., Crosbie, E. C., Moore, R. H., Herrmann, F., Oßwald, P., Wahl, C., Kapernaum, M., Köhler, M., Le Clercq, P., Rauch, B., Eichler, P., Mikoviny, T., and Wisthaler, A.: Impact of Alternative Jet Fuels on Engine Exhaust Composition During the 2015 ECLIF Ground-Based Measurements Campaign, Environmental Science amp; Technology, 52, 4969–4978, https://doi.org/10.1021/acs.est.7b06244, 2018.

Schripp, T., Anderson, B. E., Bauder, U., Rauch, B., Corbin, J. C., Smallwood, G. J., Lobo, P., Crosbie, E. C., Shook, M. A., Miake-Lye, R. C., Yu, Z., Freedman, A., Whitefield, P. D., Robinson, C. E., Achterberg, S. L., Köhler, M., Oßwald, P., Grein, T., Sauer, D., Voigt, C., Schlager, H., and LeClercq, P.: Aircraft engine particulate matter emissions from sustainable aviation fuels: Results from ground-based measurements during the NASA/DLR campaign ECLIF2/ND-MAX, Fuel, 325, 124 764, https://doi.org/10.1016/j.fuel.2022.124764, 2022.

Schumann, U., Schlager, H., Arnold, F., Baumann, R., Haschberger, P., and Klemm, O.: Dilution of aircraft exhaust plumes at cruise altitudes, Atmospheric Environment, 32, 3097–3103, https://doi.org/10.1016/s1352-2310(97)00455-x, 1998.

Shingler, T., Dey, S., Sorooshian, A., Brechtel, F. J., Wang, Z., Metcalf, A., Coggon, M., Mülmenstädt, J., Russell, L. M., Jonsson, H. H., and Seinfeld, J. H.: Characterisation and airborne deployment of a new counterflow virtual impactor inlet, Atmospheric Measurement Techniques, 5, 1259–1269, https://doi.org/10.5194/amt-5-1259-2012, 2012.

Solomon, S., Daniel, J. S., Neely, R. R., Vernier, J.-P., Dutton, E. G., and Thomason, L. W.: The Persistently Variable "Background" Stratospheric Aerosol Layer and Global Climate Change, Science, 333, 866–870, https://doi.org/10.1126/science.1206027, 2011.

Stith, J. L., Avallone, L. M., Bansemer, A., Basarab, B., Dorsi, S. W., Fuchs, B., Lawson, R. P., Rogers, D. C., Rutledge, S., and Toohey, D. W.: Ice particles in the upper anvil regions of midlatitude continental thunderstorms: the case for frozen-drop aggregates, Atmospheric Chemistry and Physics, 14, 1973–1985, https://doi.org/10.5194/acp-14-1973-2014, 2014.

https://doi.org/10.5194/egusphere-2026-2161
Preprint. Discussion started: 23 April 2026

Tang, G., Panetta, R. L., Yang, P., Kattawar, G. W., and Zhai, P.-W.: Effects of ice crystal surface roughness and air bubble inclusions on cirrus cloud radiative properties from remote sensing perspective, Journal of Quantitative Spectroscopy and Radiative Transfer, 195, 119–131, https://doi.org/10.1016/j.jqsrt.2017.01.016, laser-light and Interactions with Particles 2016, 2017.

Textor, C., Graf, H.-F., Timmreck, C., and Robock, A.: Emissions from volcanoes, in: Emissions of Atmospheric Trace Compounds, edited by Granier, C., Artaxo, P., and Reeves, C. E., pp. 269–303, Springer Netherlands, Dordrecht, ISBN 978-1-4020-2167-1, https://doi.org/10.1007/978-1-4020-2167-1_7, 2004.

Thomas, M. A., Giorgetta, M. A., Timmreck, C., Graf, H.-F., and Stenchikov, G.: Simulation of the climate impact of Mt. Pinatubo eruption using ECHAM5 – Part 2: Sensitivity to the phase of the QBO and ENSO, Atmospheric Chemistry and Physics, 9, 3001–3009, https://doi.org/10.5194/acp-9-3001-2009, 2009.

Tomsche, L., Marsing, A., Jurkat-Witschas, T., Lucke, J., Kaufmann, S., Kaiser, K., Schneider, J., Scheibe, M., Schlager, H., Röder, L., Fischer, H., Obersteiner, F., Zahn, A., Zöger, M., Lelieveld, J., and Voigt, C.: Enhanced sulfur in the upper troposphere and lower stratosphere in spring 2020, Atmospheric Chemistry and Physics, 22, 15 135–15 151, https://doi.org/10.5194/acp-22-15135-2022, 2022.

TSI: Technical Sheet Model 3340, Tech. rep., TSI Incorporated, 2017.

Twohy, C. H.: Measurements of Saharan Dust in Convective Clouds over the Tropical Eastern Atlantic Ocean, Journal of the Atmospheric Sciences, 72, 75 – 81, https://doi.org/10.1175/JAS-D-14-0133.1, 2015.

Ungeheuer, F., Caudillo, L., Ditas, F., Simon, M., van Pinxteren, D., Kılıç, D., Rose, D., Jacobi, S., Kürten, A., Curtius, J., and Vogel, A. L.: Nucleation of jet engine oil vapours is a large source of aviation-related ultrafine particles, Communications Earth & Environment, 3, https://doi.org/10.1038/s43247-022-00653-w, 2022.

Vogel, B., Günther, G., Müller, R., Grooß, J.-U., Hoor, P., Krämer, M., Müller, S., Zahn, A., and Riese, M.: Fast transport from Southeast Asia boundary layer sources to northern Europe: rapid uplift in typhoons and eastward eddy shedding of the Asian monsoon anticyclone, Atmospheric Chemistry and Physics, 14, 12 745–12 762, https://doi.org/10.5194/acp-14-12745-2014, 2014.

Voigt, C., Schumann, U., Minikin, A., Abdelmonem, A., Afchine, A., Borrmann, S., Boettcher, M., Buchholz, B., Bugliaro, L., Costa, A., Curtius, J., Dollner, M., Dörnbrack, A., Dreiling, V., Ebert, V., Ehrlich, A., Fix, A., Forster, L., Frank, F., Fütterer, D., Giez, A., Graf, K., Grooß, J.-U., Groß, S., Heimerl, K., Heinold, B., Hüneke, T., Järvinen, E., Jurkat, T., Kaufmann, S., Kenntner, M., Klingebiel, M., Klimach, T., Kohl, R., Krämer, M., Krisna, T. C., Luebke, A., Mayer, B., Mertes, S., Molleker, S., Petzold, A., Pfeilsticker, K., Port, M., Rapp, M., Reutter, P., Rolf, C., Rose, D., Sauer, D., Schäfler, A., Schlage, R., Schnaiter, M., Schneider, J., Spelten, N., Spichtinger, P., Stock, P., Walser, A., Weigel, R., Weinzierl, B., Wendisch, M., Werner, F., Wernli, H., Wirth, M., Zahn, A., Ziereis, H., and Zöger, M.: ML-CIRRUS: The Airborne Experiment on Natural Cirrus and Contrail Cirrus with the High-Altitude Long-Range Research Aircraft HALO, Bulletin of the American Meteorological Society, 98, 271–288, https://doi.org/10.1175/bams-d-15-00213.1, 2017.

Voigt, C., Kleine, J., Sauer, D., Moore, R. H., Braeuer, T., Clercq, P. L., Kaufmann, S., Scheibe, M., Jurkat-Witschas, T., Aigner, M., Bauder, U., Boose, Y., Borrmann, S., Crosbie, E., Diskin, G. S., DiGangi, J., Hahn, V., Heckl, C., Huber, F., Nowak, J. B., Rapp, M., Rauch, B., Robinson, C., Schripp, T., Shook, M., Winstead, E., Ziemba, L., Schlager, H., and Anderson, B. E.: Cleaner burning aviation fuels can reduce contrail cloudiness, Communications Earth & Environment, https://doi.org/10.1038/s43247-021-00174-y, 2021.

Voigt, C., Lelieveld, J., Schlager, H., Schneider, J., Curtius, J., Meerkötter, R., Sauer, D., Bugliaro, L., Bohn, B., Crowley, J. N., Erbertseder, T., Groß, S., Hahn, V., Li, Q., Mertens, M., Pöhlker, M. L., Pozzer, A., Schumann, U., Tomsche, L., Williams, J., Zahn, A., Andreae, M., Borrmann, S., Bräuer, T., Dörich, R., Dörnbrack, A., Edtbauer, A., Ernle, L., Fischer, H., Giez, A., Granzin, M., Grewe, V., Harder, H., Heinritzi, M., Holanda, B. A., Jöckel, P., Kaiser, K., Krüger, O. O., Lucke, J., Marsing, A., Martin, A., Matthes, S., Pöhlker, C., Pöschl, U., Reifenberg, S., Ringsdorf, A., Scheibe, M., Tadic, I., Zauner-Wieczorek, M., Henke, R., and Rapp, M.: Cleaner Skies during the

https://doi.org/10.5194/egusphere-2026-2161
Preprint. Discussion started: 23 April 2026

COVID-19 Lockdown, Bulletin of the American Meteorological Society, 103, E1796–E1827, https://doi.org/10.1175/bams-d-21-0012.1, 2022.

Voigt, C., Märkl, R., Sauer, D., Dischl, R., Kaufmann, S., Bräuer, T., Jurkat, T., Renard, C., Seeliger, K., Chenadec, G. L., Moreau, J., Yu, F., Bonne, N., Roche, A., Zelina, J., Dörnbrack, A., Eirenschmalz, L., Heckl, C., Horst, E., Lichtenstern, M., Marsing, A., Roiger, A., Scheibe, M., Stock, P., Giez, A., Eckel, G., Neumann, G., Vals, M., Requena-Esteban, E., and Clercq, P. L.: Substantial aircraft contrail formation at low soot emission levels, https://doi.org/10.21203/rs.3.rs-6559440/v1, 2025.

von Glasow, R., Bobrowski, N., and Kern, C.: The effects of volcanic eruptions on atmospheric chemistry, Chemical Geology, 263, 131–142, https://doi.org/10.1016/j.chemgeo.2008.08.020, halogens in Volcanic Systems and Their Environmental Impacts, 2009.

Wang, X., Randel, W., Pan, L., Wu, Y., and Zhang, P.: Transient Behavior of the Asian Summer Monsoon Anticyclone Associated With Eastward Eddy Shedding, Journal of Geophysical Research: Atmospheres, 127, https://doi.org/10.1029/2021jd036090, 2022.

Weisenstein, D. K., Visioni, D., Franke, H., Niemeier, U., Vattioni, S., Chiodo, G., Peter, T., and Keith, D. W.: An interactive stratospheric aerosol model intercomparison of solar geoengineering by stratospheric injection of SO_2 or accumulation-mode sulfuric acid aerosols, Atmospheric Chemistry and Physics, 22, 2955–2973, https://doi.org/10.5194/acp-22-2955-2022, 2022.

Woiwode, W., Dörnbrack, A., Bramberger, M., Friedl-Vallon, F., Haenel, F., Höpfner, M., Johansson, S., Kretschmer, E., Krisch, I., Latzko, T., Oelhaf, H., Orphal, J., Preusse, P., Sinnhuber, B.-M., and Ungermann, J.: Mesoscale fine structure of a tropopause fold over mountains, Atmospheric Chemistry and Physics, 18, 15 643–15 667, https://doi.org/10.5194/acp-18-15643-2018, 2018.

Wylie, D. P. and Menzel, W. P.: Eight Years of High Cloud Statistics Using HIRS, Journal of Climate, 12, 170 – 184, https://doi.org/10.1175/1520-0442(1999)012<0170:EYOHCS>2.0.CO;2, 1999.

Yu, F., Anderson, B. E., Pierce, J. R., Wong, A., Nair, A., Luo, G., and Herb, J.: On Nucleation Pathways and Particle Size Distribution Evolutions in Stratospheric Aircraft Exhaust Plumes with H2SO4 Enhancement, Environmental Science & Technology, 58, 6934–6944, https://doi.org/10.1021/acs.est.3c08408, pMID: 38651174, 2024.

Yu, P., Toon, O. B., Bardeen, C. G., Zhu, Y., Rosenlof, K. H., Portmann, R. W., Thornberry, T. D., Gao, R.-S., Davis, S. M., Wolf, E. T., de Gouw, J., Peterson, D. A., Fromm, M. D., and Robock, A.: Black carbon lofts wildfire smoke high into the stratosphere to form a persistent plume, Science, 365, 587–590, https://doi.org/10.1126/science.aax1748, 2019.

Yu, Z., Herndon, S. C., Ziemba, L. D., Timko, M. T., Liscinsky, D. S., Anderson, B. E., and Miake-Lye, R. C.: Identification of Lubrication Oil in the Particulate Matter Emissions from Engine Exhaust of In-Service Commercial Aircraft, Environmental Science & Technology, 46, 9630–9637, https://doi.org/10.1021/es301692t, 2012.

Zelenyuk, A. and Imre, D.: Single Particle Laser Ablation Time-of-Flight Mass Spectrometer: An Introduction to SPLAT, Aerosol Science and Technology, 39, 554–568, https://doi.org/10.1080/027868291009242, 2005.